END
DATE
FILMED
6-78
DDC

Scope

The journal is concerned with research in the field of ship technology as well as marine technology in general. This is understood here to encompass ship and other marine structures, sea loads, ship propulsion, materials engineering, yard production technique, oceanography, etc. The journal will also cover applied research within shipping economics, social science and other areas related to the marine environment.

417 283

CONTENTS

1

Sloshing loads due to random pitch motion

by

Jan Mathisen, Research Engineer, Research Division,
Det norske Veritas

Abstract

The results of model tests to determine sloshing loads due to random pitch motion are presented. A relatively long tank model is considered, and loads are measured on a deck transverse and a transverse bulkhead. A series of tests are performed with different pitch excitations, representing a large variety of short-term sea states. The short-term results are combined to give long-term distributions for sloshing loads.

1. Introduction

A prerequisite for the efficient design of ship structures is an accurate knowledge of the loads to which the structures will be exposed. One type of structural load is caused by liquid sloshing in partially-filled tanks. Satisfactory analytic methods for the calculation of sloshing loads are not available; sloshing is therefore mainly investigated by means of model tests. Det norske Veritas has recently acquired a ship motion simulator with six degrees of freedom, with a view to obtaining better data concerning sloshing loads. This paper describes some of the first model tests performed using the simulator in random motion.

The primary objective of these tests was to obtain long-term sloshing loads on a deck transverse and on a transverse bulkhead in a relatively long oil cargo tank, under random pitch excitation. Secondary objectives were to investigate techniques for motion excitation and for the analysis of test data.

2. Model tests

2.1 Tank Models

The basic tank model was intended to represent an oil cargo centre tank, situated amidships, with length equal to one-fifth of the ship length. The ship was considered to be transversely framed, with moulded depth one-tenth of the ship length. A sec-
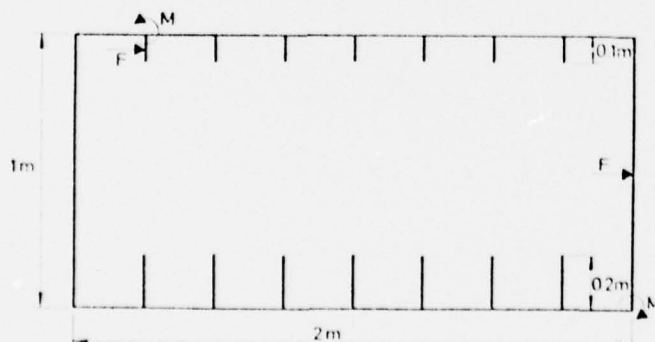
Fig 1. Longitudinal section through basic tank model (tank 5). Dimensions are in model scale.
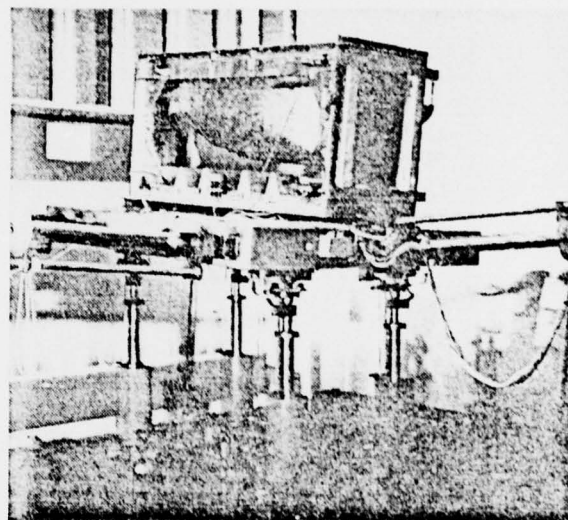
Fig. 2. Tank model mounted on ship motion simulator.

Table 1. Tank arrangements

TANK NO	ℓ (m)	D/ℓ	b/ℓ	s/ℓ	NO OF BOTTOM TRANSVERSES	d_0/ℓ	d_1/ℓ
2	1.25	0.8	0.56	0.125	7	0.1	0.05
5	2	0.5	0.35	0.125	7	0.1	0.05
6	2	0.5	0.35	0.083	11	0.1	0.05
7	2	0.5	0.35	0.125	7	0.05	0.05

7 deck transverses in each tank.
No stringers present on the bulkheads.

tion through the basic tank model is shown in fig. 1, and fig. 2 shows the tank mounted on the ship motion simulator.

The tank was constructed with interchangeable elements, allowing different arrangements of internal structure. The arrangements used in the present tests are indicated in Table 1. In addition, a relatively short tank was included for comparison in a few

tests. Further details of the models are given in reference [1].

2.2 Model Scaling

The experiments were designed for Froude and geometric scaling. Froude scaling was necessary to allow for free surface effects. Other effects were neglected; viz. viscosity, surface tension, liquid compressibility, cavitation and tank elasticity.

Assuming a ship length of 250 m, the full scale tank length (for tanks 5, 6, 7) was 50 m, and the geometric scale was 1/25. The time scale is the square root of the geometric scale; i.e. 1/5.

2.3 Filling Height

The results presented herein were all obtained with the tanks 75 % full ($h/D = 0.75$). Previous harmonic tests had shown that this filling height gave the most severe loads on the deck transverse and transverse bulkhead. This filling ($h/\ell = 0.375$, tanks 5, 6, 7) corresponds quite well to the filling ($h/\ell = 0.31$) theoretically calculated to give maximum surface elevation in an open rectangular tank [2]. For the short tank (tank No. 2), however, the theoretical height-to-length ratio indicates that a lower filling depth ($h/D = 0.43$) would be likely to give greater sloshing loads.

2.4 Pitch Excitation

Excitation was applied to the tanks in the form of pitch motion only. The centre of rotation was located in the centre of the tanks. Other forms of motion were not expected to produce significant sloshing loads on the structural components under consideration.

The excitation was required to represent random ship pitching under different sea states. A wide range of sea states was chosen to roughly cover the sea states likely to be encountered in a ship lifetime. Six average apparent wave periods were selected, each with three significant wave heights, giving a total of eighteen different sea states. Pitch spectra were calculated for each sea state using DnV computer programs [3, 4]. The calculations were based on the Series 60 hull form, with block coefficient 0.8, as being representative of typical tankers. Zero ship speed and head seas were considered to prevail under conditions of extreme pitching.

The ship motion simulator was used to give the tank the appropriate pitch motion. It can simulate pitch angles with amplitudes up to 10°. A short description of the simulator may be found in [5]. The long term distribution of pitch angle (fig. 3) indicates that a maximum pitch angle of 10° is ample for ships over 200 m in length.

A pitch time history must be supplied to the simulator, for the generation of command signals to the hydraulic cylinders controlling the platform motion. Fig. 4 indicates the two techniques used to supply the motion history. The analogue mode was chosen for the present tests because this is convenient when only one degree of freedom is required. Six band pass filters were designed to correspond to the pitch

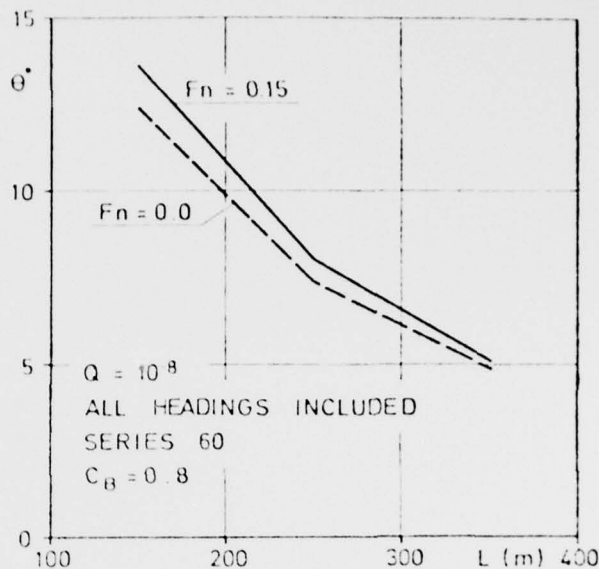Fig. 3. Long term distribution of pitch angle, based on North Atlantic wave statistics.

spectra for the various wave periods. The calibrated potentiometer (fig. 4) was used to adjust the pitch amplitude with respect to the significant wave height.

Fig. 5 shows a comparison between a calculated pitch spectrum and the spectrum produced by one of the filters. The filters were designed to give the same
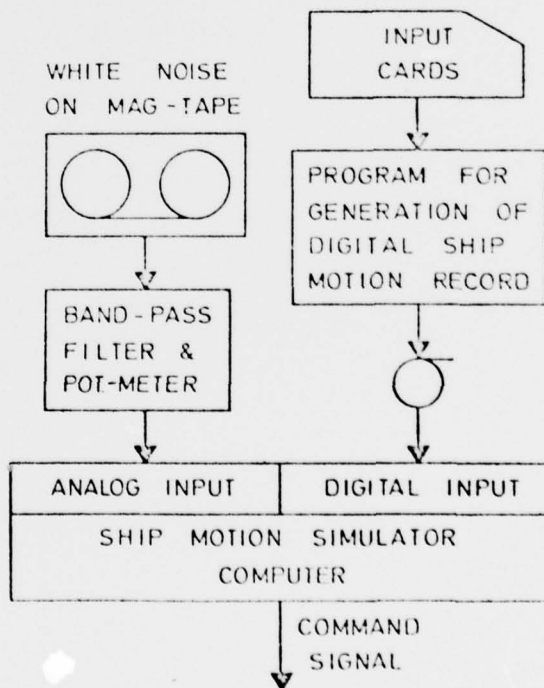

Fig. 4. Motion excitation.

3

spectral width and period of peak pitch intensity. Table 2 gives a comparison of calculated and simulated spectral parameters. The simulated pitch spectra were considered to be suitable for the present experiments, but better agreement with analytic spectra could have been obtained by using more sophisticated analogue filters, or with digital simulation.

Table 2. Comparison of calculated and simulated pitch spectra.

CALCULATED			
$\bar{T}\sqrt{g/L}$	$T_p\sqrt{g/L}$	$T_z\sqrt{g/L}$	ξ
0 2.05	2.74	2.60	0.34
1 2.33	3.03	2.76	0.37
2 1.84	2.61	2.46	0.32
3 1.47	2.36	2.19	0.29
4 1.28	2.13	2.02	0.28
5 1.11	1.83	1.83	0.26

FILTER NO.	SIMULATED		
0	2.70	2.35	0.62
1	2.92	2.27	0.70
2	2.49	2.14	0.65
3	2.35	2.08	0.60
4	2.11	1.87	0.54
5	1.95	1.72	0.49

The variance (σ^2) of the pitch angle was measured for each of the 18 excitation conditions. Pitch angle maxima are Rayleigh-distributed in the short term; i.e. for a constant sea state:

$$E = 2\sigma^2 \tag{1}$$

$$P(\theta \leq X) = 1 - \exp(-X^2/E) \tag{2}$$

The most probable largest pitch angles (θ_M) during each test (one hour) could then be found (table 3).

Table 3. Excitation levels for simulated pitch spectra.

Filter no.	Level 1		Level 2		Level 3	
	σ^2 (RAD^2)	θ_M (DEG.)	σ^2 (RAD^2)	θ_M (DEG.)	σ^2 (RAD^2)	θ_M (DEG.)
0	.000163	2.8	.000652	5.6	.00147	8.4
1	.000156	2.7	.000623	5.5	.00140	8.2
2	.000127	2.5	.000508	5.0	.00114	7.5
3	.000116	2.4	.000465	4.8	.00105	7.2
4	.000102	2.2	.000407	4.5	.000915	6.7
5	.000098	2.2	.000392	4.4	.000881	6.6

Fig. 6 shows the short term response parameter for pitch as a function of wave period, calculated with computer program NV406 [6]. For a chosen ship length (L = 250 m), the significant wave
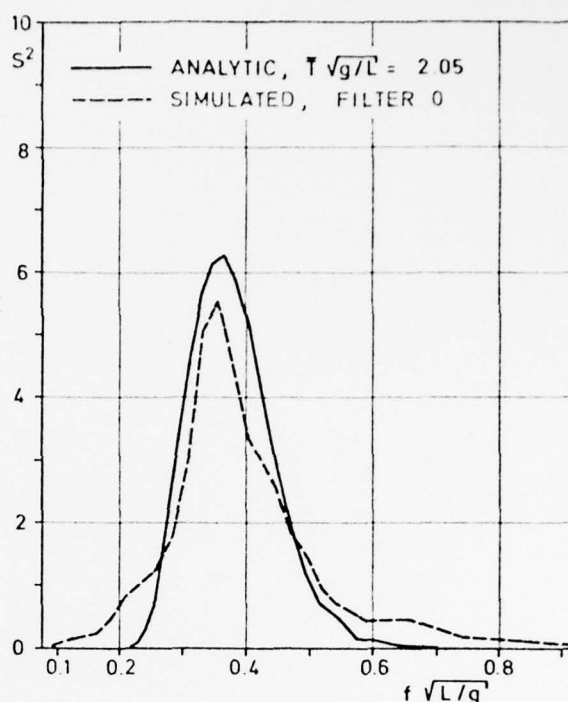
Fig. 5. Comparison of analytic and simulated pitch spectra.

heights $(H_{1/3})$ corresponding to the simulated pitch time histories were then calculated:

$$H_{1/3} = 4\sigma/[\sqrt{8E}/(H_{1/3}/L)] \cdot L \tag{3}$$

Significant wave heights are given in Table 4. A few of these wave heights are unrealistic, but the corresponding pitch conditions may give realistic values of wave height for other ship lengths.

Table 4. Significant wave heights (L = 250 m)

EXCITATION LEVEL	1	2	3
FILTER NO.	$H_{1/3}$(m)	$H_{1/3}$(m)	$H_{1/3}$(m)
0	5.50	10.9	16.4
1	5.33	10.6	15.9
2	5.15	10.3	15.5
3	6.47	13.0	19.5
4	8.35	16.6	25.0
5	12.7	25.4	38.1

2.5 Model Instrumentation

One transvere bulkhead and one deck transverse were each attached to the tank by means of 4 force transducers. Necessary sealing of the tank was accomplished by means of flexible rubber diaphragms. This arrangement allowed the measure-

1

ment of total force (F) and moment (M) on these two structural members (fig. 1).

Fig. 7 shows the arrangement used to record the responses. Since only 4 channels were available on the analogue tape recorder, the moment on the bulkhead was omitted. Previous harmonic tests had shown the force to be fairly evenly distributed on the bulkhead, thus allowing the estimation of moment from force.
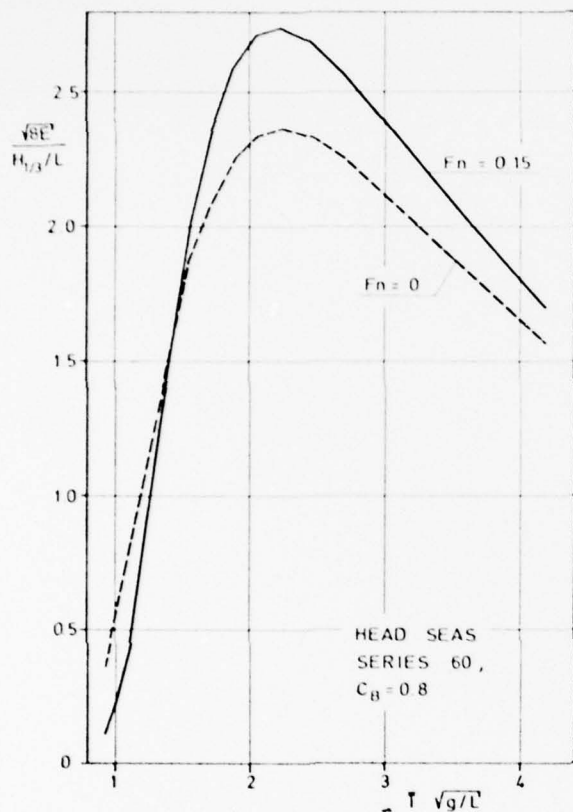
Fig. 6. Short-term response, pitch.

Fig. 7. Recording response.

Fig. 8. Typical test record.

1 Pitch angle.

2 Force on deck transverse.

3 Moment on deck transverse.

4 Force on transverse bulkhead.

3. Data reduction

3.1 Digitisation

A typical test record is shown in fig. 8, and fig. 9 shows a «quicker» view of force on the deck transverse. The duration of this force is about 1/20 second in model scale.

Somewhat different procedures were necessary to analyse slowly varying responses such as pitch, and «impulsive» responses such as force on the deck transverse. The initial sampling and digitisation took place in DnV's datalab. The dataflow is shown in fig. 10. The peak detector was used to detect the peak values of responses of very short duration. Its principle of operation is illustrated in fig. 11. The comparator level is pre-set to avoid the registration of false peaks due to noise. When the input exceeds the comparator level the following peak is held.

After a short delay a pacer pulse is separately transmitted to the computer, commanding the digitisation of the peak value.

5

0.95 s (MODEL SCALE)
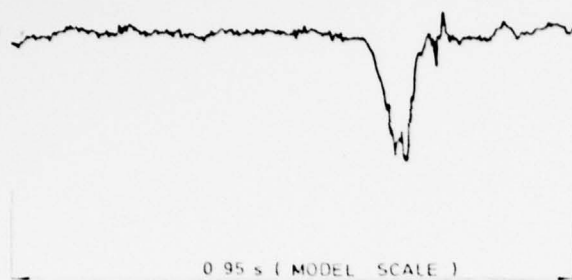
Fig 9. Force on deck transverse.
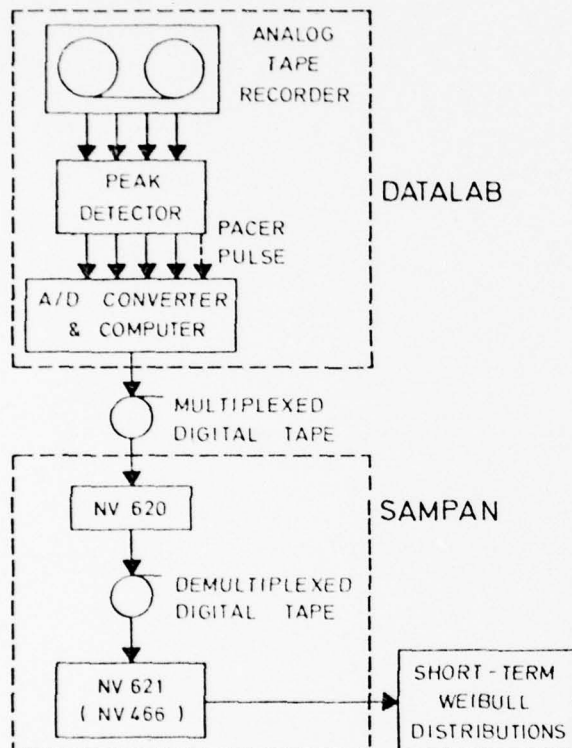
Fig. 10. Response analysis.

INPUT

COMP LEVEL

OUTPUT

PACER
PULSE

TIME

PEAK DETECTOR

Fig. 11. Peak detector.

ment was constructed from each set of peak values. The probabilities were related to the number of pitch cycles (N) in each test.

$$N = t/T_z \tag{4}$$

Number of responses recorded above level $X = n$

$$Q(x > X) = n/N \tag{5}$$

Program NV466 /9/ was incorporated in NV621 in order to fit Weibull distributions to the experimental probability distributions. The Weibull distribution is written:

$$Q(x > X) = \exp(-(X/A)^M) \tag{6}$$

Program NV466 uses a least squares technique to find values of the slope parameter (M) and the scale parameter (A). In some cases, NV466 did not yield satisfactory results and the Weibull distribution was fitted manually.

3.3 Long term distribution

Long-term distributions of the sloshing load (Q_{LT}) were obtained by combining the short-term distribution (Q_{ST}) with allowance for their probability of occurrence.
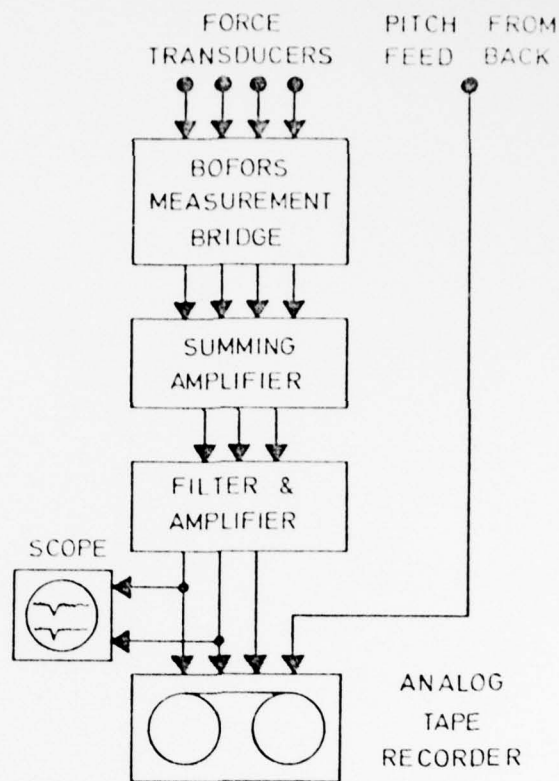
$$Q_{LT}(\cdot > X) = \sum_{i=1}^{m}$$

$$Q_{ST_i}(\cdot > X | T, H_{1/3}) \cdot P(H_{1/3} | T) \cdot P(T) \tag{7}$$

The probability of occurrence of each short-term distribution was obtained from the probability of

Peak values for force and moment on the deck transverse were digitised together, as they occured practically simultaneously. The peak detector was also used for force on the transverse bulkhead, but not for pitch angle, which was digitised at evenly spaced time instants. The digitised values were stored on magnetic tape.

3.2 Short-term Analysis

A program set known as «SAMPAN» was used for the analysis of the digitised data on a UNIVAC 1110 computer. Demultiplexing of data was performed by program NV620 /7/, while NV621 /8/ carried out analysis according to specified directives. Spectral analysis was applied to the pitch records. An experimental probability distribution for force or mo-

6

occurrence of the sea states $(\bar{T}, H_{1/3})$ producing the pitch excitation. These probabilities were determined from wave statistics for the North Atlantic /10/.

The experimentally determined short-term Weibull distributions were used in the above summation, and the long-term probabilities of exceedance (Q_{LT}) were calculated for a series of values of slosh load (X). Finally, a Weibull distribution function was fitted to the calculated distribution.

4. Results

4.1 Short-term Results for Deck Transverse

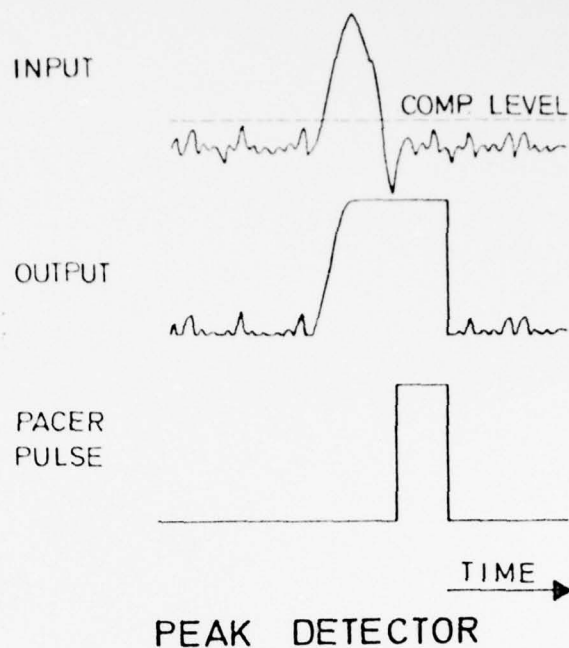Short-term distributions for force on the deck transverse are plotted on Weibull probability paper in figs. 12 and 13. It can be seen that the observed probabilities are well represented by the fitted straight lines. Fig. 12 illustrates the effect of variation in the excitation level, while fig. 13 shows the variation with excitation spectrum. The same type of results was obtained for moment on the deck transverse. On average about 500 slosh loads were observed at excitation level 3, 350 loads at level 2 and 200 slosh loads at level 1 in each test. This means that the short-term distributions were less accurately determined at the lowest excitation level. Insufficient data were obtained at excitation level 1 in some cases, and Weibull parameters were interpolated from adjacent results. Complete results are given in Tables 5 and 6, and in Table 7 for the short tank (No. 2). Inspection of the tables shows that the scale parameter (A) increases as the excitation level increases. The same tendency generally appears for the slope parameter (M), because the probability of an impact against the deck transverse increases with the excitation level. However, very large values of M occur at excitation level 1 in several cases. This may be due to inaccuracies.
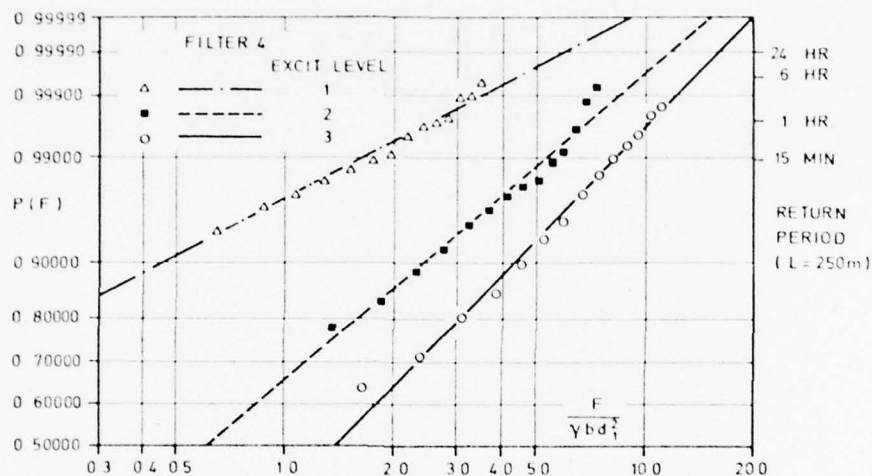

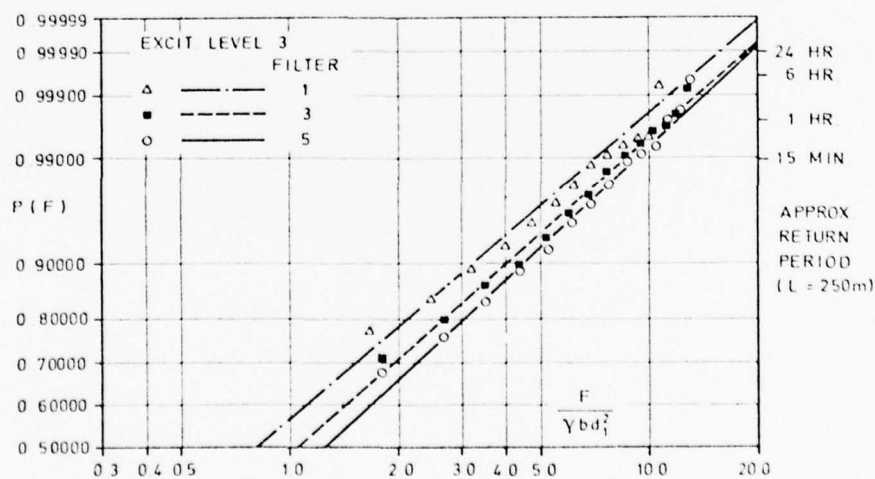Fig. 12. Short-term distribution, Force on deck transverse, tank 6.

Fig. 13. Short-term distribution, Force on deck transverse, tank 6.

7

TANK		5 MOD		5		6		7	
FILTER	EXCIT LEVEL	A	M	A	M	A	M	A	M
0	1	0.189	2.810	0.212	1.180	0.024	0.455	0.0040*	0.445
	2	0.215	0.558	0.225	0.568	0.557	0.730	0.196	0.660
	3	0.813	0.693	1.087	0.861	1.329	0.892	0.950	0.858
1	1	0.306	1.189	0.293	1.207	0.015*	0.455		
	2	0.176	0.508	0.225	0.611	0.472	0.721	0.196	0.605
	3	0.968	0.741	1.160	0.853	1.235	0.860	0.625	0.566
2	1	0.155	2.450	0.156	3.524	0.023	0.455	0.012	0.445
	2	0.195	0.655	0.350	0.632	0.465	0.702	0.285	0.706
	3	1.179	0.810	1.156	0.941	1.296	0.816	0.713	0.686
3	1	0.516*	2.450	0.358	3.524	0.059	0.455	0.016	0.445
	2	0.695	0.894	0.549	0.731	0.726	0.882	0.310	0.703
	3	1.485	0.745	1.718	0.987	1.578	0.885	0.925	0.738
4	1	0.067	0.521	0.040	0.538	0.094	0.525	0.063	0.564
	2	0.831	0.753	0.919	0.886	0.930	0.859	0.539	0.717
	3	1.735	0.749	1.980	0.993	1.598	1.010	1.184	0.882
5	1	0.040	0.455	0.014	0.332	0.141	0.589	0.156	0.667
	2	0.715	0.785	0.550	0.879	0.509	0.795	0.788	0.804
	3	1.879	0.888	1.950	0.976	1.825	0.936	2.277	1.185

* Interpolated

Table 6. Short-term Weibull parameters.
Moment on deck transverse $M/(\gamma b\, d_1^{\,3})$

TANK		5 MOD		5		6		7	
FILTER	EXCIT LEVEL	A	M	A	M	A	M	A	M
0	1	0.143	2.930	0.150	2.070	0.0017*	0.516		
	2	0.185	0.554	0.325	0.828	0.140	0.602	0.103	0.675
	3	0.629	0.862	0.820	1.040	0.428	0.757	0.390	0.751
1	1	0.093*	2.930	0.222	2.700				
	2	0.138	0.576	0.205	0.731	0.097	0.573	0.073	0.547
	3	0.630	0.815	0.790	1.000	0.351	0.672	0.295	0.678
2	1	0.139	1.940	0.150	4.080	0.011*	0.516	0.029*	0.814
	2	0.380	0.897	0.210	0.628	0.128	0.576	0.122	0.629
	3	0.720	0.864	0.650	0.924	0.411	0.711	0.320	0.653
3	1	0.288*	1.940	0.033	0.751	0.018	0.516	0.019	0.814
	2	0.495	1.000	0.450	0.868	0.185	0.695	0.148	0.676
	3	1.330	1.020	1.050	1.010	0.500	0.734	0.440	0.714
4	1	0.062	0.604	0.020	0.483	0.024	0.468	0.069	0.752
	2	0.159	0.834	0.700	1.080	0.270	0.686	0.320	0.804
	3	0.933	0.753	1.300	1.200	0.646	0.849	0.570	0.707
5	1	0.038	0.593			0.067	0.627	0.105	0.765
	2	0.400	0.805	0.590	0.976	0.287	0.704	0.400	0.799
	3	0.940	0.874	1.180	0.959	0.604	0.749	0.936	0.890

* Interpolated.

Table 7. Short-term Weibull Parameters.
Loads on tank 2 (short tank).
Excitation level 3.

FILTER		4		5	
LOAD		A	M	A	M
FORCE ON DECK TRANSVERSE $\dfrac{F}{\gamma b\, d_1^{\,2}}$		0.227	1.162	0.280	1.280
MOMENT ON DECK TRANSVERSE $\dfrac{M}{\gamma b\, d_1^{\,3}}$		0.185	1.620	0.180	1.470
FORCE ON BULKHEAD $\dfrac{F}{\gamma b\, D^2}$		0.023	2.589	0.023	1.731

Loads on the deck transverse in the short tank were about one-tenth of the loads in the other tanks. It was difficult to draw conclusions concerning the relative magnitudes for tanks 5, 6 and 7. However, one tendency was clear; namely that 11 bottom transverses (tank 6) gave greater forces than 7 bottom transverses (tank 5). At probability of exceedance, $Q = 10^{-3}$, the forces on the deck transverse were, on average, 6% greater at excitation level 2, and 13% greater at excitation level 3. This seems to indicate that very closely spaced bottom transverses provide less effective damping of sloshing.

4.2 Modification of Tank 5

As the experiments progressed, some uncertainty arose concerning the effect on the sloshing loads of leakage between the deck transverse and tank top. The rubber sealing lip employed was somewhat long and flexible. The deck transverse was therefore modified as shown in fig. 14, and the tests repeated for tank 5. The results thus obtained are referred to as «Tank 5 MOD». Results for tank 5 and tank 5 MOD. were compared at probability levels $Q = 10^{-2}$, 10^{-3}, and 10^{-4}, for excitation levels 2 and 3. Negligible differences were found at excitation level 2, while about 20% increase was found at level 3 for force and moment on the deck transverse. The difference increased as the probability of exceedance (Q) fell. It was deduced that the rubber seal allowed significant leakage when the sloshing loads were high. Weibull exponents corrected for this effect are given in Table 8.
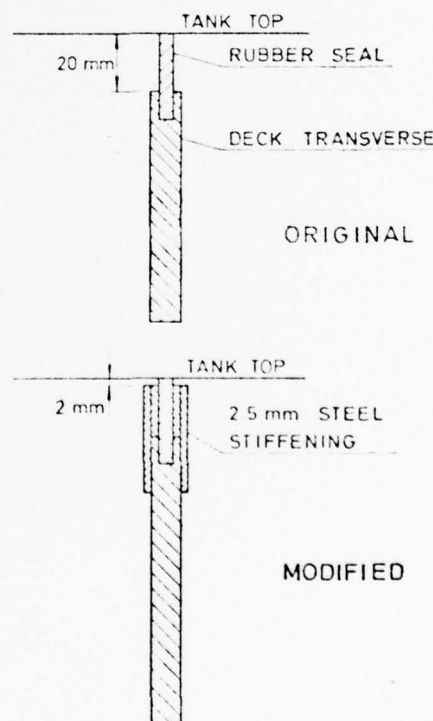
Fig. 14. Section through deck transverse (model scale).

Table 8. Corrected short-term Weibull exponent force and moment on deck transverse.

		FORCE $\dfrac{F}{\gamma b\, d_1^2}$		MOMENT $\dfrac{M}{\gamma b\, d_1^3}$	
	TANK	6	7	6	7
FILTER	EXCIT LEVEL	M	M	M	M
0	3	0.779	0.753	0.686	0.706
1	3	0.754	0.601	0.616	0.621
2	3	0.720	0.617	0.648	0.600
3	3	0.776	0.659	0.667	0.651
4	3	0.889	0.771	0.761	0.645
5	3	0.812	0.993	0.680	0.794

4.3 Short-term Results for Transverse Bulkhead

Short-term distributions for force on the transverse bulkhead are plotted on Weibull probability paper in figs. 15 and 16. The effect of variation of excitation level is shown in fig. 15, while fig. 16 shows the very slight variation with excitation spectrum. About 1000 slosh loads were used in the determination of each pair of short-term Weibull parameters, giving quite good accuracy. Tests at excitation level
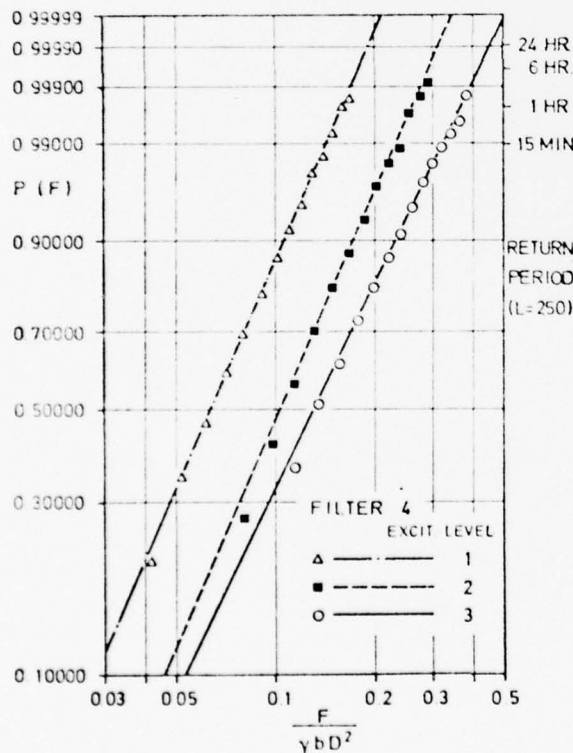

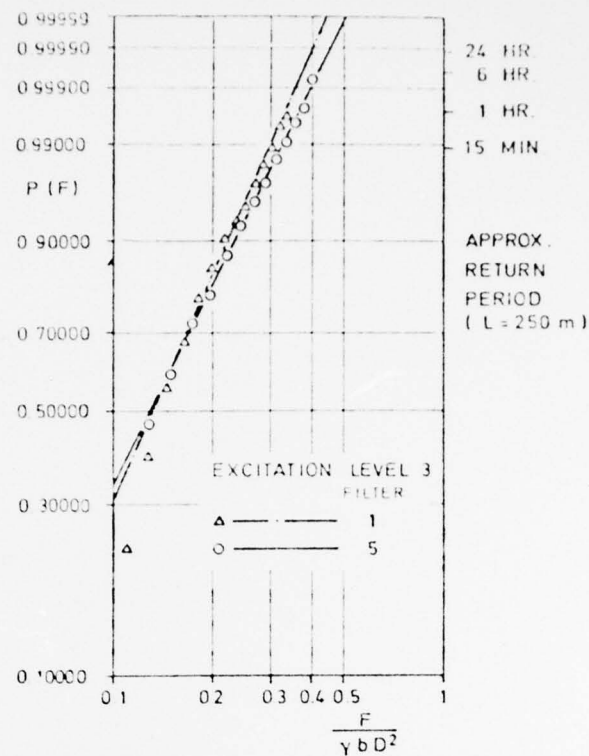Fig. 16. Short-term distribution, Force on transverse bulkhead tank 6.

Fig. 15. Short-term distribution, Force on transverse bulkhead tank 6.

Table 9. Short-term Weibull parameters. Force on bulkhead $F/(\gamma b\, D^2)$

TANK		5 MOD.		6		7	
FILTER	EXCIT LEVEL	A	M	A	M	A	M
0	1	0.056*	2.416	0.064*	2.043	0.055*	2.790
	2	0.098	2.363	0.114	2.563	0.093	2.332
	3	0.123	1.709	0.148	2.016	0.136	2.320
1	1	0.051	2.407	0.064*	2.043	0.051	2.790
	2	0.100	2.177	0.114	2.733	0.095	2.461
	3	0.145	2.135	0.152	2.316	0.132	2.231
2	1	0.060	2.416	0.064	2.043	0.058	2.790
	2	0.105	2.145	0.103	2.143	0.106	2.737
	3	0.134	2.283	0.147	2.117	0.150	2.383
3	1	0.059	2.584	0.066	2.167	0.058	2.729
	2	0.108	2.513	0.110	2.060	0.106	2.619
	3	0.142	2.070	0.155	2.443	0.154	2.519
4	1	0.071	2.690	0.074	2.323	0.066	2.705
	2	0.095	2.092	0.121	2.317	0.114	2.738
	3	0.126	1.760	0.157	2.089	0.156	2.467
5	1	0.057	2.119	0.082	2.395	0.067	2.894
	2	0.101	2.054	0.117	2.353	0.117	2.557
	3	0.131	2.037	0.153	2.058	0.182	2.982

* Interpolated.

1 were omitted in a few cases, and Weibull parameters were interpolated from adjacent results. Complete results are given in Table 9, and in Table 7 for the short tank (No. 2). Note that the slope

parameter (M) has values close to 2.0. This corresponds to the Rayleigh distribution function which generally applies to wave-induced loads that vary linearly with excitation.

Short-term results were compared at probability of exceedance, $Q = 10^{-3}$. Bulkhead forces in the short tank (No. 2) were about 1/6 of the forces in the other tanks, however, a lower filling level would probably give greater loads in the short tank (c.f. § 2.3). Increasing the number of bottom transverses from 7 (Tank 5 MOD.) to 11 (Tank 6) gave an increase in force of 25 % at excitation level 1, 9 % at level 2 and 6 % at level 3. Halving the height of the bottom transverses (Tank 7) reduced the forces 8 % on average for all excitation levels.

4.4 Long-term Distributions
Long-term distributions of sloshing loads have been calculated for Tank 5 MOD. Figs. 17 and 18 show the loads on the deck transverse. Note that the slope of the curves, indicated by the Weibull parameter M, is small. This parameter is important when considering the accuracy of the results. If $M = 0.3$, then an in-

accuracy of 3 % in the determination of M will lead to 25 % inaccuracy in the load at probability level, $Q = 10^{-8}$. However, if $M = 1.0$, then 3 % error in the determination of M will give only 8 % error in the load at $Q = 10^{-8}$. The above reasoning, together with the inaccurate short-term distributions at excitation level 1, indicates that the present long term distributions for force and moment on the deck transverse are of low accuracy.

Fig. 19 gives the long-term distribution for force on the transverse bulkhead. This result is not considered to suffer from the same inaccuracies as the loads on the deck transverse.

The long-term distributions presented in this article correspond to a ship length of 250 m. However, the short-term experimental results could equally well have been used for other ship lengths.

4.5 Use of Results
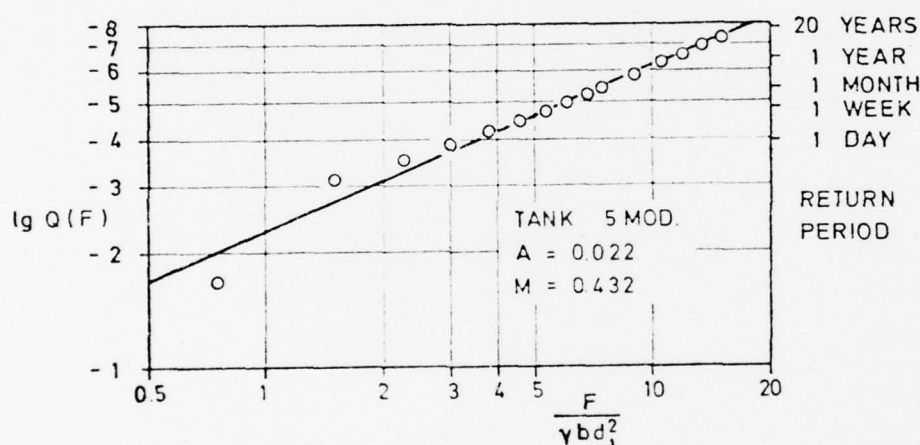As an example, a ship of 250 m length has been considered, with an amidships centre tank of 50 m

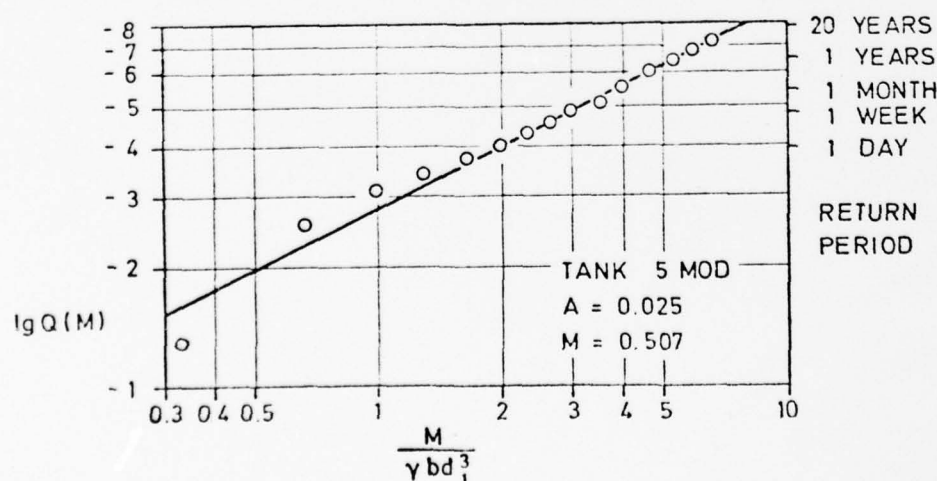Fig. 17. Long-term distribution, force on deck transverse, L = 250 m.

Fig. 18. Long-term distribution, moment on deck transverse, L = 250 m.

length. The ship was assumed to sail a total of 2 years under North Atlantic weather conditions with the tank 75 % full, corresponding to a probability level of about $Q = 10^{-7}$

The long-term load distributions were based on an average pitch period of 11.1 sec. Using this period, the number of pitch cycles (N) in two years were found:

$$N = 10^{6.75} \tag{8}$$

$$\therefore Q = 1/N = 10^{-6.75} \tag{9}$$

The dimensionless loads were extracted from the Weibull distributions at this probability of exceedance:

Deck transverse $\begin{cases} F/(\gamma bd_1^2) = 12.3 & (10) \\ M/(\gamma bd_1^3) = 5.69 & (11) \end{cases}$

Transverse bulkhead $\quad F/(\gamma bD^2) = 0.348 \tag{12}$

Pressures corresponding to the deck transverse loads are shown in fig. 20. These pressures are very large. A reduction in the time spent with 75 % full tank could reduce them considerably. Some reduction should also be expected when allowance is made for motion with six degrees of freedom. The short duration (about 1/4 sec. in full scale) should be taken into account when applying these pressures to the deck transverse.

The bulkhead force corresponds to a uniform pressure of 8.8 T/m². A specific weight (γ) of 1 T/m³ was assumed for liquid in the tank when calculating these pressures.

Extreme sloshing loads were also estimated from the short term results. Fig. 3 indicates a pitch angle of 7.4° at $Q = 10^{-8}$ and zero ship speed. At $Q = 10^{-7}$ seven-eighths of this value are obtained; i.e. a pitch angle of 6.5°. Applying the Rayleigh distribution for pitch angle, with filter 2 and excitation level 3, showed this angle to be the most probable largest in 274 pitch cycles, or about 1 hour. The probability of exceedance was thus:

$$Q = 1/274 = 10^{-2.44} \tag{13}$$

Sloshing loads were extracted from the short-term distributions for filter 2 and excitation level 3 at this probability level.

Deck transverse $\begin{cases} F/(\gamma bd_1^2) = 9.94 \\ M/(\gamma bd_1^3) = 5.31 \end{cases}$

Transverse bulkhead $\quad F/(\gamma bD^2) = 0.286$

These dimensionless loads are less than the largest loads recorded in the model tests, so that extrapolation of the short-term distributions has not been necessary to obtain them. Corresponding pressures on the deck transverse are shown in fig. 20. The bulkhead force corresponds to a uniform pressure of 7.1 T/m². Mean pressures based on the short-term results are about 20 % less than obtained from the long-term results.

5. Conclusion

Model tests have been carried out to measure sloshing loads on a deck transverse and transverse bulkhead in a 75 % full cargo tank, under pitch excitation. The tests were, in general, successful, but of too short duration at the lowest pitch excitation level. This resulted in inaccurate short-term distributions for loads on the deck transverse at this
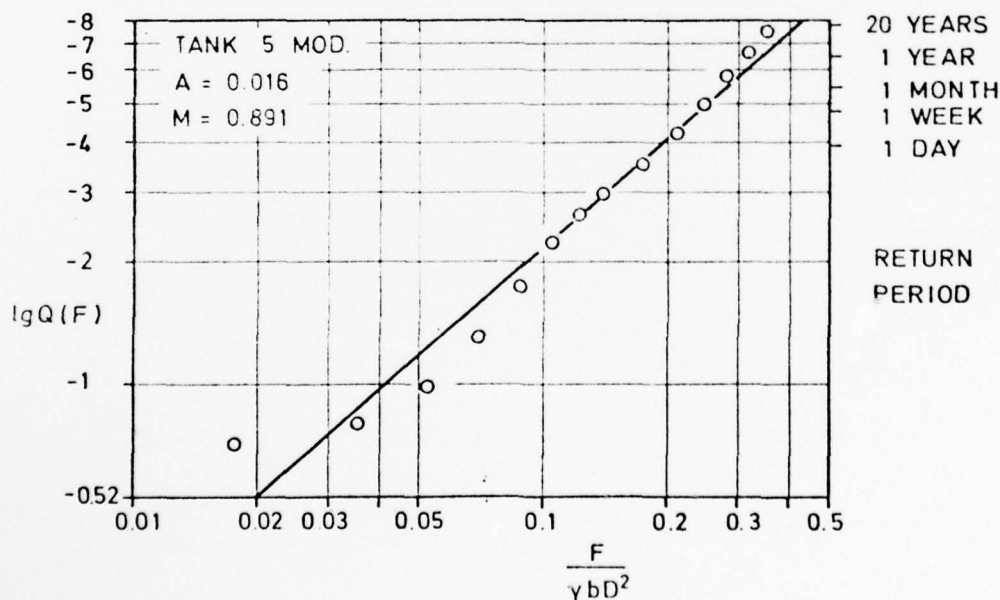
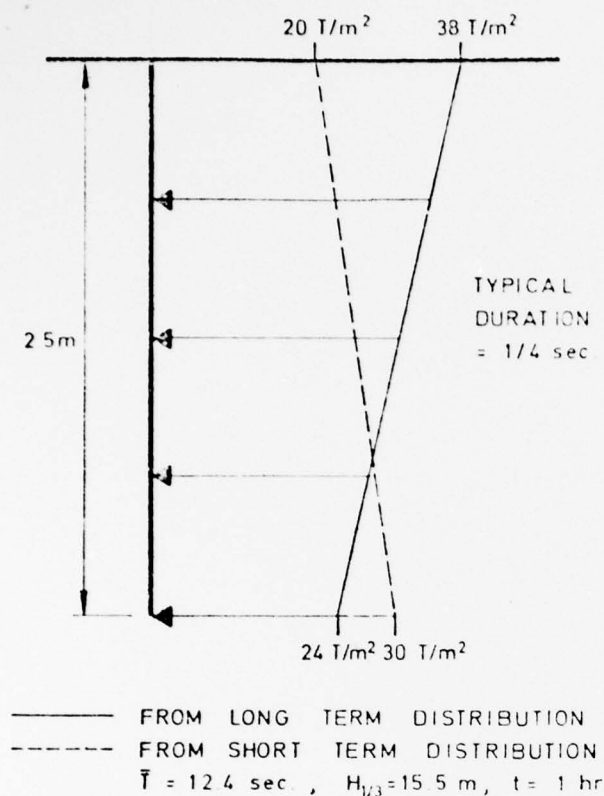Fig. 19. Long-term distribution, force on transverse bulkhead, L = 250 m

11

20 T/m² 38 T/m²

TYPICAL
DURATION
= 1/4 sec

2.5 m

24 T/m² 30 T/m²

———— FROM LONG TERM DISTRIBUTION
- - - - - FROM SHORT TERM DISTRIBUTION
$\bar{T}$ = 12.4 sec , $H_{1/3}$ = 15.5 m, t = 1 hr

Fig. 20. Most probable largest load on deck
transverse in 2 years ($Q = 10^?$, $\theta = 6.5°$)
L = 250 m, ℓ/L = 20 %, h/D = 0.75,
TANK 5 MOD.

excitation level. The Weibull distribution function
gave a good fit to the observed load distributions.

Comparison of the dimensionless short-term re-
sults for various tank configurations gave the fol-
lowing results:

(i) Loads on the deck transverse in the short tank
(ℓ = 1.25 m) were about one-tenth of the loads
in the long tanks (ℓ = 2 m). The short tank
represents current designs with tank length
about 1/10 of the ship length, while the long
tank illustrates the effect of the trend towards
longer tanks.
(ii) Forces on the transverse bulkhead in the short
tank were about one-sixth of the forces in the
long tank. The force on the transverse bulkhead
in the long tank corresponds to about 70 % of
the static force when the tank is full.
(iii) 11 bottom transverses resulted in greater slosh-
ing loads than 7 bottom transverses.
(iv) High bottom transverses (d_0/ℓ = 0.1) gave
greater forces on the bulkhead than low bottom
transverses (d_0/ℓ = 0.05).

Long term distributions of sloshing loads have
been calculated for one tank configuration and a
ship length of 250 m. The method presented appears
to have produced reasonable long-term distributions,
both for the impulsive loads on the deck trans-

verse, and for the slower-varying force on the trans-
verse bulkhead. However, inaccuracies in the short-
term distributions for loads on the deck transverse
at low excitation are expected to have produced
significant inaccuracies in the corresponding long-
term distributions. This inaccuracy does not apply
to force on the bulkhead.

6. Acknowledgement

7. References

1. DIDRIKSEN, T.:
   Two tanks for sloshing tests. Design and instru-
   mentation.
   DnV report No. 75-269.
2. FALTINSEN, O., OLSEN, H., ABRAMSON, H.,
   BASS, R.:
   Liquid Slosh in LNG Carriers. 10th Symp. on
   Naval Hydrodynamics, Boston, June 1974.
3. FALTINSEN, O.:
   Computer program specification NV417. Second
   Edition. Wave induced ship motions and loads.
   Six degrees of freedom.
   DnV report No. 74-19-S.
4. GRAN, S.:
   Computer program specification NV421. Simu-
   lation of waves and ship responses.
   DnV report No. 72-12-S.
5. RIMEID, B. E.:
   Det norske Veritas Ship Motion Simulator.
   Veritas No. 76, October 1973.
6. LØKEN, A. E.:
   Computer program specification NV406.
   Short and long-term response of wave-induced
   motions and loads.
   DnV report No. 74-22-S.
7. OMUNDSEN, T. A., and MOI, K.:
   User's Manual for NV620 SAMPAN.
   Retrieval of raw data from an Analogue-Digital
   Conversion.
   Computas Report No. 74-34.
8. LEREN, P. O., and HAUGERUD, M. H.:
   User's documentation for NV621 SAMPAN.
   Analysis of measured data from oscillatory ex-
   periments (in Norwegian).
   Computas report No. 74-35.
9. MATHISEN, J.:
   Computer program specification NV466.
   Fitting of Weibull Probability Distributions to
   Observed Data.
   DnV report No. 74-7-S.
10. WALDEN, H.:
    Die Eigenschaften der Meereswellen im Nord-
    Atlantischen Ozean. Statistik 10-jähriger See-
    gangs-beobachtungen der Nordatlantischen
    Ozean-Wetterschiffe.
    Deutscher Wetterdienst, Seewetteramt, Einzel-
    veröffentlichungen Nr. 41, Hamburg, 1964.

8. Notation

A	Weibull scale parameter	N	number of pitch cycles
b	tank breadth	p	probability of occurrence
C_B	block coefficient	P	probability that load level will not be exceeded
d_o	depth of bottom transverse	Q	probability of exceedance
d_1	depth of deck transverse		suffix ST indicates short-term
D	tank depth ($\approx$ ship depth)		suffix LT indicates long-term
E	short-term Rayleigh parameter	s	spacing of bottom transverses
f	frequency (H_z)	S^2	normalised pitch variance intensity
F	force (on deck transverse or bulkhead)	t	time (duration of test in seconds)
F_n	dimensionless Froude number for ship speed	$\bar{T}$	average apparent wave period
g	acceleration due to gravity	T_p	period corresponding to peak of pitch spectrum
h	tank filling height	T_z	pitch zero-up-crossing period
$H_{1/3}$	significant wave height	X	randomly chosen sloshing load
i	summation index	X	sloshing load level
ℓ	tank length		
L	ship length	γ	specific weight of liquid in tank
m	number of short-term sea states	σ_o^2	variance of pitch angle
M	moment on deck transverse	θ	pitch angle
M	Weibull slope parameter	θ_M	most probable largest pitch angle
n	number of sloshing loads exceeding level X	ξ	spectral width

---

Stress analysis of longitudinal/girder connections

by

K. Haslum[1], K. Kristoffersen[2] and L. A. Andersen[3]
[1] Aker Group, [2] Det norske Veritas and [3] Fredriksstad Mek. Verksted

Abstract

**The detail structural design of the intersection between a longtitudi-
nal stiffener and a transverse girder has been analysed by the finite
element method. Stress concentration factors are given for alternative
designs together with practical design recommendations.**

Introduction

The design of the intersection of a longitudinal and
a transverse is usually regarded as a detail design
problem, and until recently has not received too
much attention by the classification societies. Each
yard has to some extent followed its own standard.
Various designs of different qualities have been
used. Only a few of them have been subject to ex-
tensive investigations /1/.

The purpose of the work described here was to
evaluate the various designs in order to arrive at
some guidelines for choosing a good standard de-
sign.

Damage statistics from tankers show that up to
80 % of cracks that had to be repaired occurred at
the connection between a longitudinal stiffener and
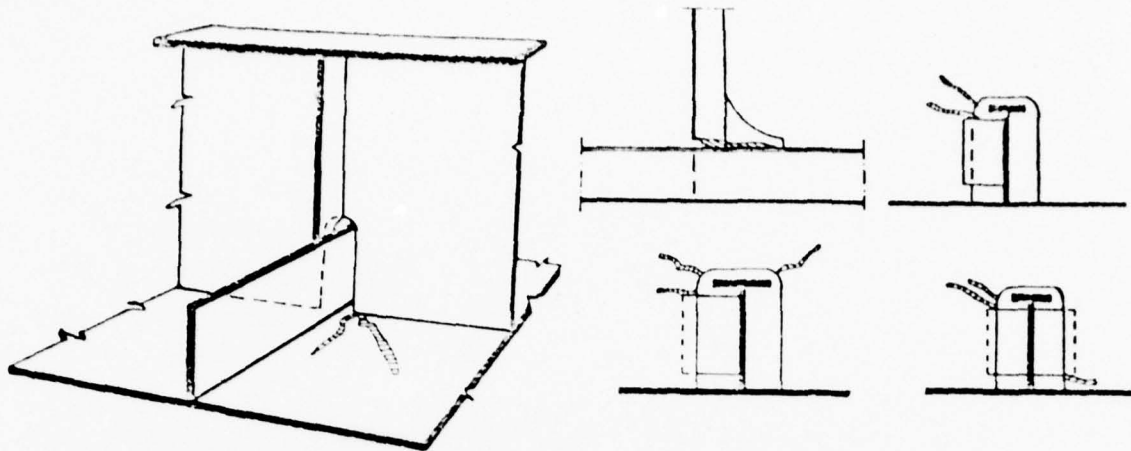a transverse girder fig. 1 /2/.

Fig 1. Typical Damages /5/

Another interesting fact is that the frequency of damages is much higher for tankers than for dry cargo ships although the maximum static stress level is practically the same in both. This may be due to the alternating load on the longitudinal/girder connections for tankers, fig. 2.
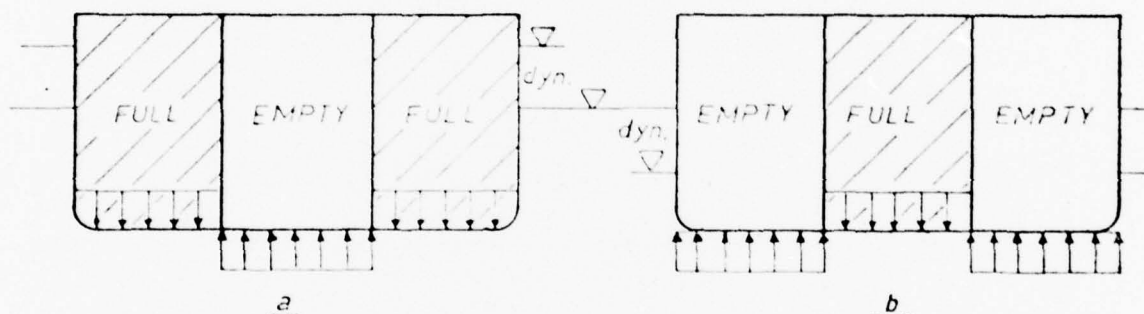

Fig. 2. Two loading conditions (incl. wave action) that may cause yielding in a longitudinal/girder connection.

The maximum values of the pressure difference from outside and inside respectively give stresses of approximately the same magnitude. If now the stress concentration factor is large enough to give yielding for one of the loading cases, the other case may cause reverse yielding (hysteresis). Reversed yielding of this type leads to fatigue fracture after relatively few cycles (1000–10000) — low cycle fatigue.

Method of analysis

The finite element program (ISODOF) which is used for this analysis is described in /3/ where also a listing of the program is given.

Compatible, quadrilateral isoparametric, linear strain finite elements with 16 degrees of freedom /1/ were used throughout in the investigation, in order to obtain the best possible accuracy with a minimum of effort. It is practical to distinguish the force transferred from each stiffener, P, from the overall shear force, Q, in the girder, fig. 3.

11

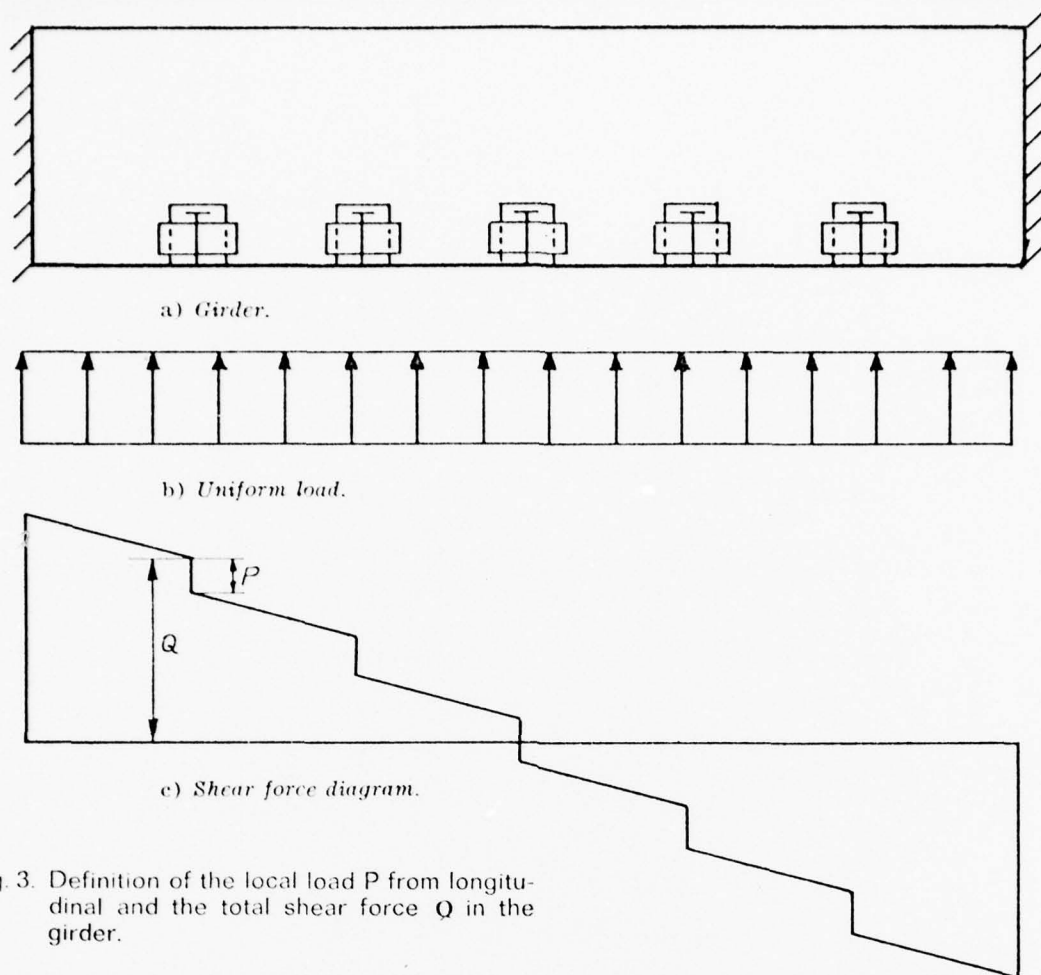a) *Girder.*

b) *Uniform load.*

c) *Shear force diagram.*

Fig. 3. Definition of the local load P from longitu-
dinal and the total shear force Q in the
girder.

At an early stage in the work a coarse element
mesh, fig. 4 b, covering the greater part of a girder
length was used to find the overall stress distribu-
tion, fig. 6, and the stiffness reduction, fig. 5, of a
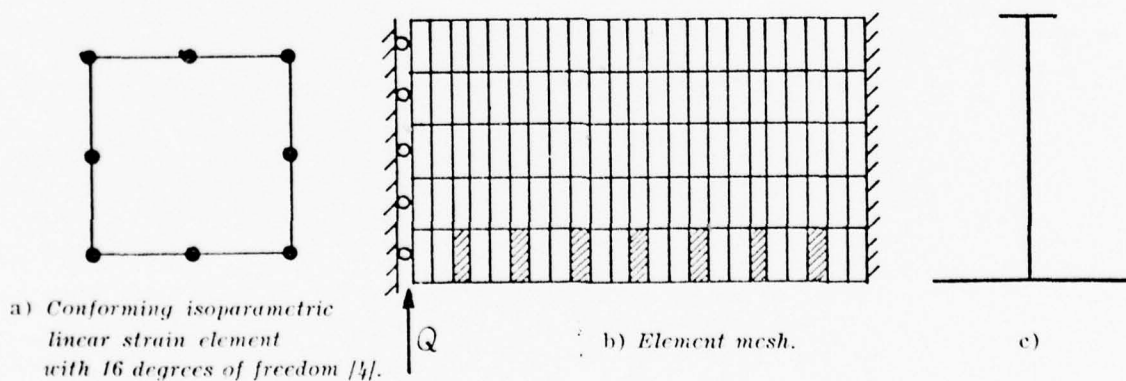girder with cutouts.

a) *Conforming isoparametric
linear strain element
with 16 degrees of freedom /4/.*

b) *Element mesh.*

c)

Fig. 4. FEM Model used to give the overall stress
distribution and the stiffness reduction of
a girder with cutouts.

15

The reduction in bending stiffness of the girder due to the cutouts is negligible. The shear stiffness, however, is considerably reduced. The reduction of shear stiffness is considerably higher than the percentage reduction in the shear area might indicate, fig. 5.
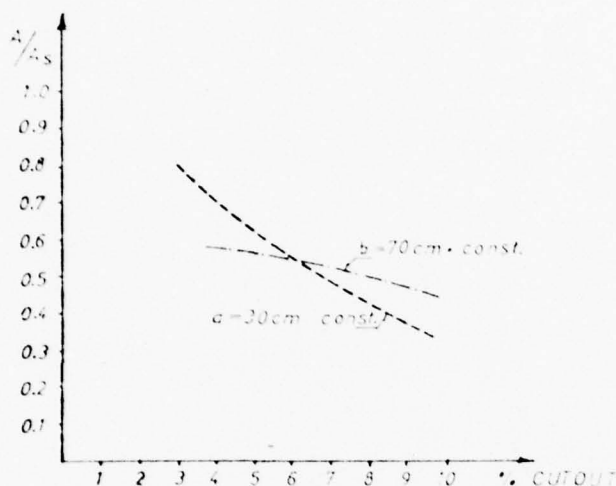
Fig. 5. Reduction in effective shear area A_S as a function of cutout ratio.

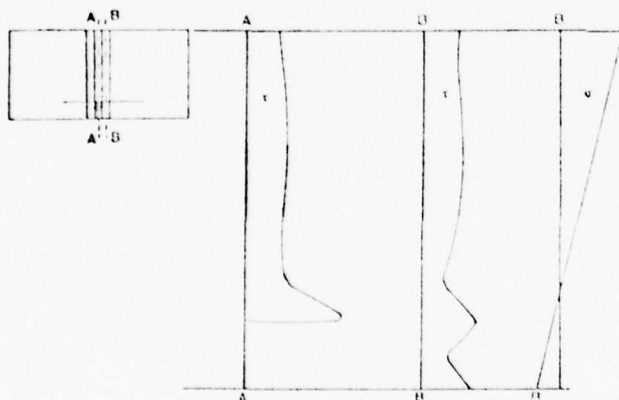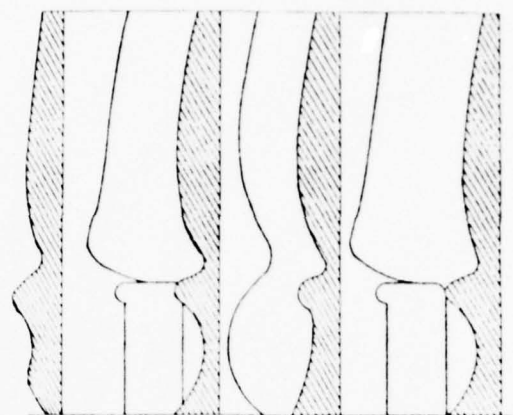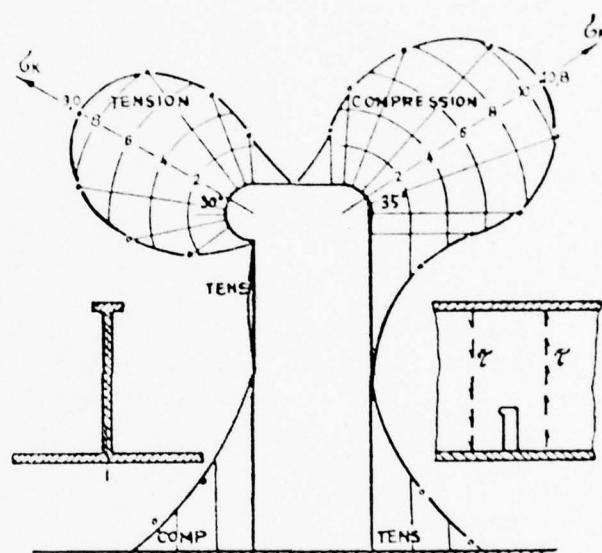The shear and bending stress distributions in section A and B, fig. 6, gave good correlation with the experimental results obtained by Gibzstein /1/, fig. 7.

Fig. 6 Stress distributions obtained by the finite element analysis.

a) *Shear stress distribution obtained by experimental analysis /1/.*


b) *Tangential boundary stress.*

Fig. 7. Similar results from photoelastic analysis performed by M. Gibzstein /1/.

The coarse mesh model in fig. 4 b was used to obtain the most realistic loading and boundary conditions, fig. 8, for the finer mesh detail models in figs. 9—12.

The largest stresses in the girder or the connection are caused by the overall shear force in the girder or by the force transferred from the longitudinal, or by their combination.
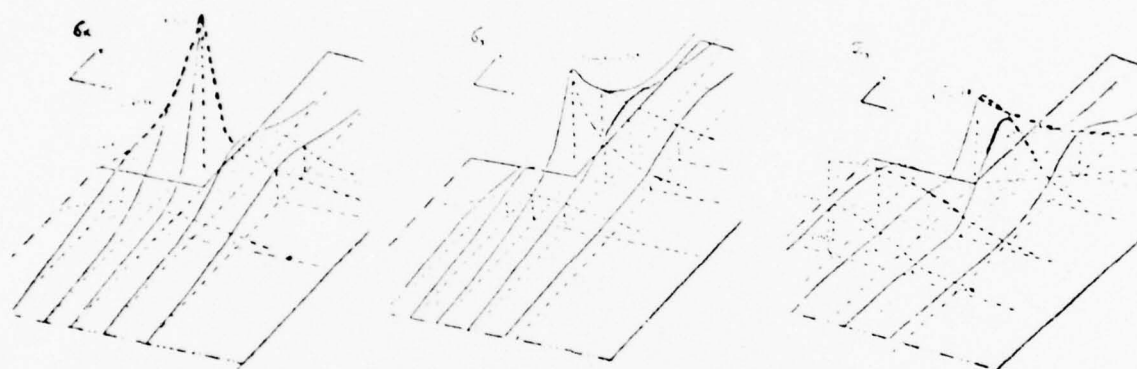
The relative significance of these loads varies along the girder.

In order to make the results applicable in more general cases, these two loading cases were treated separately.
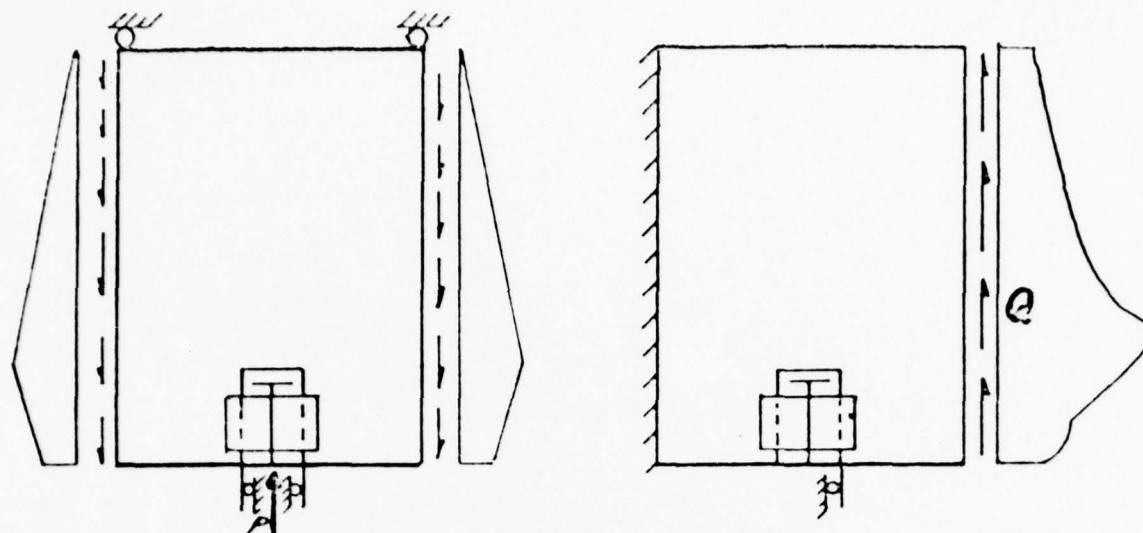
a) *Force transfer from longitudinal.*   **b)** *Total shear force in girder.*

c) *Typical stress distributions near the upper
corner of the longitudinal.*

Fig. 8. Boundary conditions and loading cases.

The stress concentration factor in the upper corner of the cutout, fig. 9, is found as a function of the corner radius. Results are shown in fig. 13.

Special attention was paid to regions with large strain gradients, where the mesh had to be fine. With small modifications the element model could be used with different parameter values. Other types of longitudinal/girder connections required separate finite element meshes, fig. 10, 11, 12, with breadths equal to the longitudinal spacing and with one half on each side of the cutout. This is necessary when analysing asymmetrical cutouts. The dimensions of the calculation model correspond to a transverse web in the bottom of a 100–150 000 dwt tanker.

In the finite element calculations it was assumed that the lug/web connection would remain in plane during loading (a two-dimensional FEM model was used). In a real structure, however, due to the lug/web configuration, there will be out-of-plane bending, giving rise to local bending stresses.

Plate bending will reduce the stiffness. A reduction in the in-plane (membrane) stresses will take place in areas with high in-plane stresses. On the contrary, bending stresses will be superimposed on the membrane stresses. These effects were investigated by three-dimensional FEM, fig. 14, and by experimental stress analysis [8]. The results show that two-dimensional FEM yields results very much in accordance with the experimental data as regards
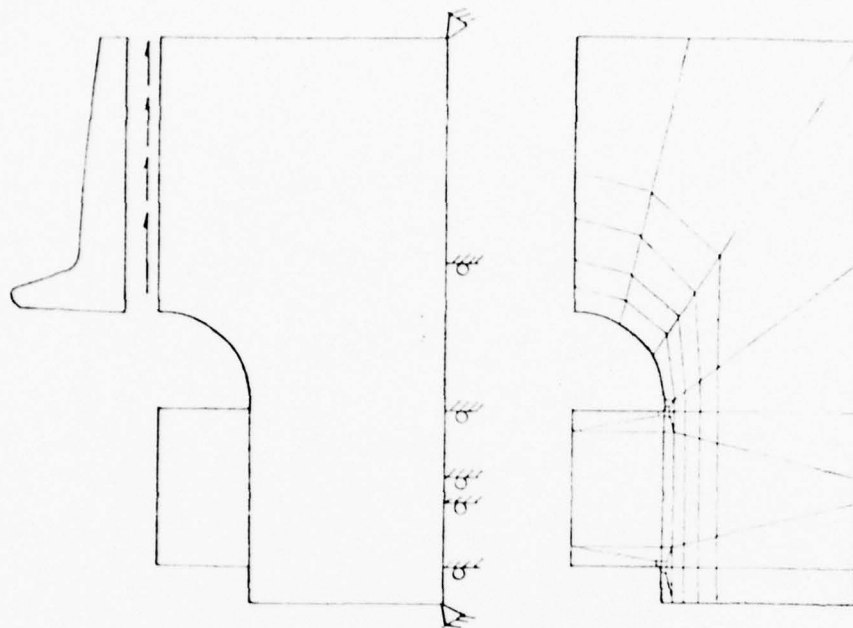
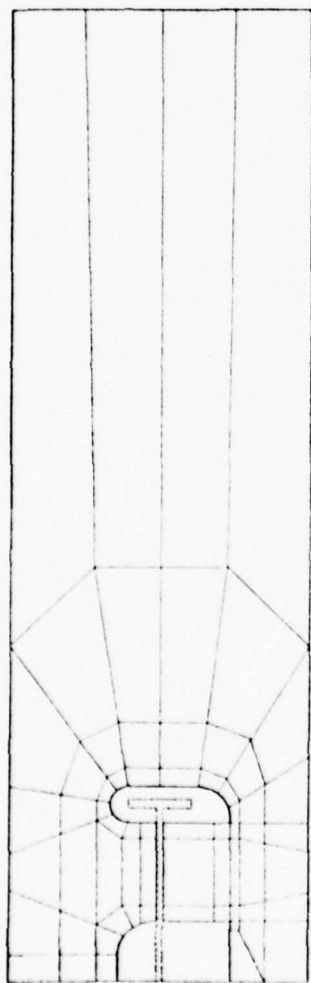17

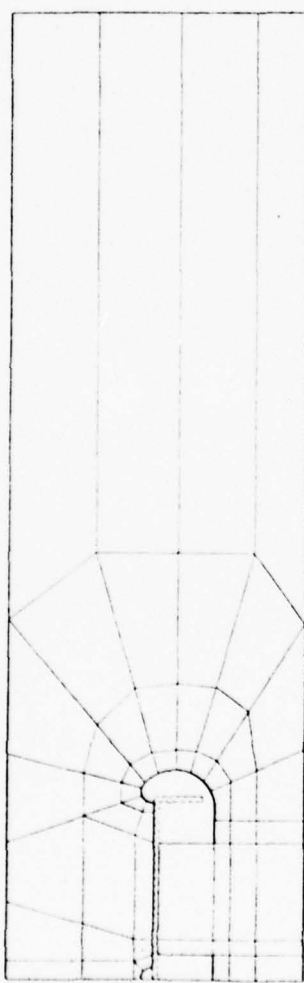Fig. 9. Boundary condition, load and finite element mesh.

Fig. 10   Fig. 11   Fig. 12

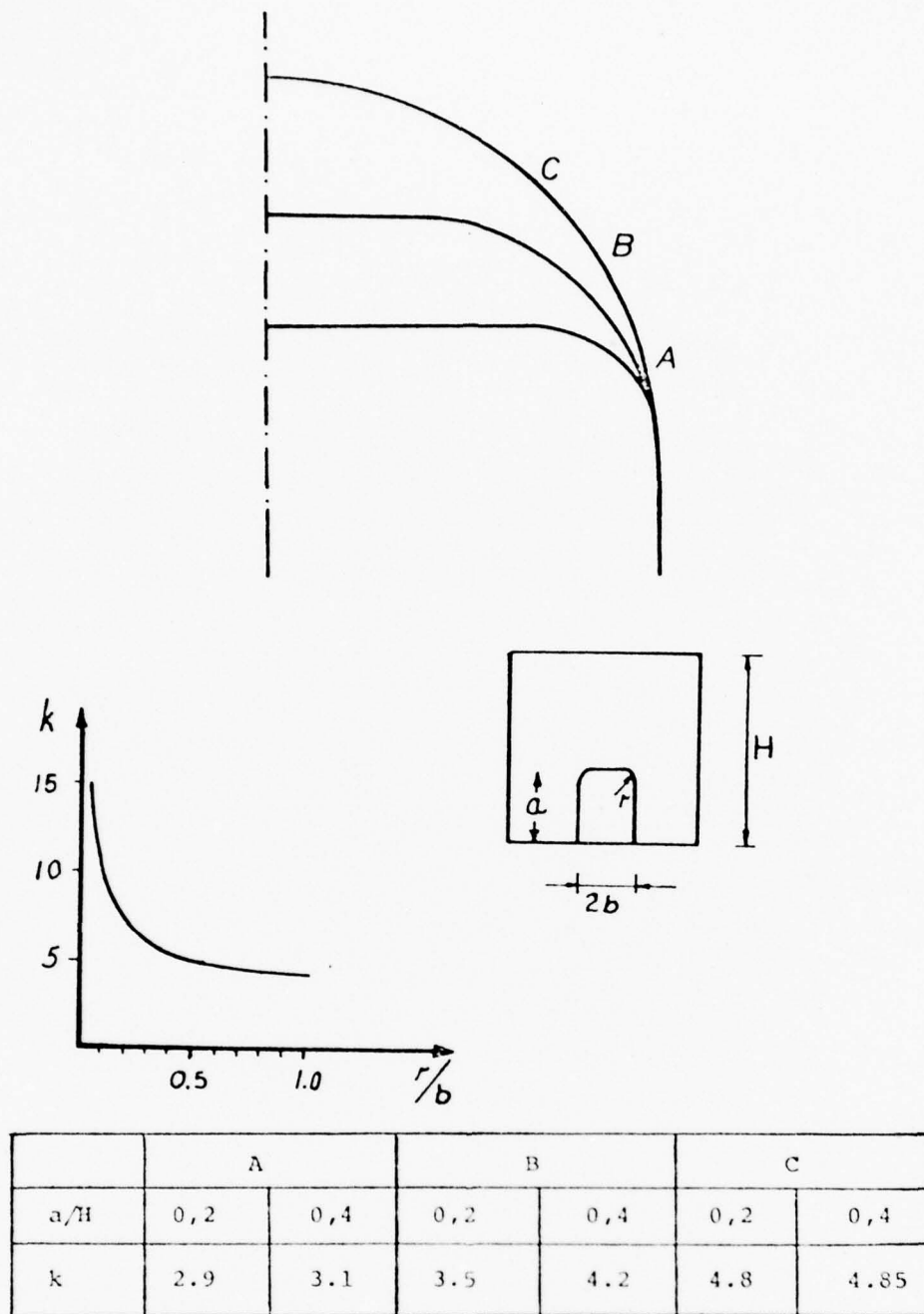|	A		B		C	
a/H	0,2	0,4	0,2	0,4	0,2	0,4
k	2.9	3.1	3.5	4.2	4.8	4.85

Fig. 13. The corner radius should preferably be
larger than a quarter of the cutout width.
The stress distribution is not very sensi-
tive to the height of the cutout as long as
this value is less than half the girder
height.

the average (membrane) stresses of the plate.

However, local bending stresses may give a signi-
ficant contribution. This is shown in fig. 15 for the
one-sided lug and fig. 16 for the lug/web connection.

This does not alter the qualitative conclusions
obtained in this report regarding design recommen-
dations for the longitudinal/girder connection. The
designer should, however, be aware of the fact that
local bending may be superimposed on the calculated
results given herein, and consider this when desig-
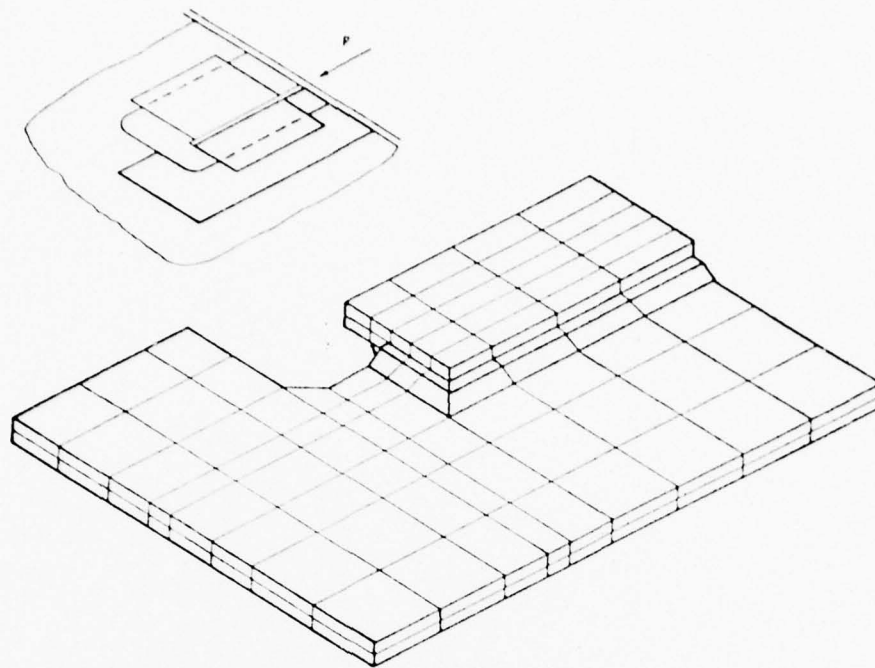ning the welded joints.

19

Fig. 14. Three-dimensional FEM model /9/ of lug/ web connection using solid eight-nodal «brick» elements /4/. Boundary conditions were taken from the two-dimensional analysis.
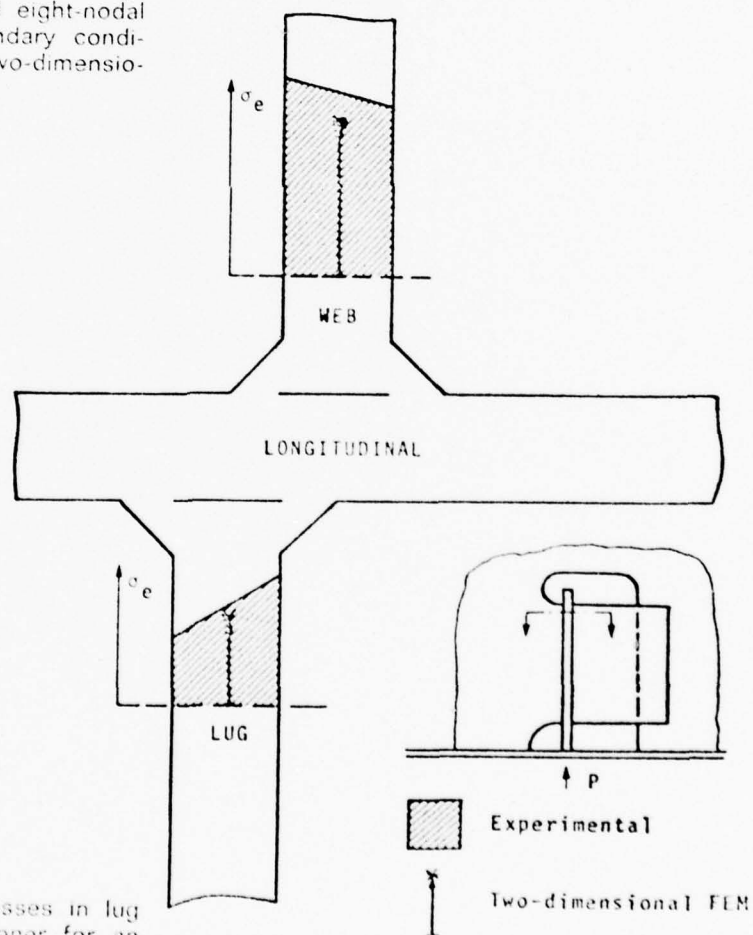

Fig 15 Equivalent (von Mises) stresses in lug and web close to the stiffener for an asymmetrical lug/web connection, from ref. /8/. The load is applied vertically through the longitudinal.
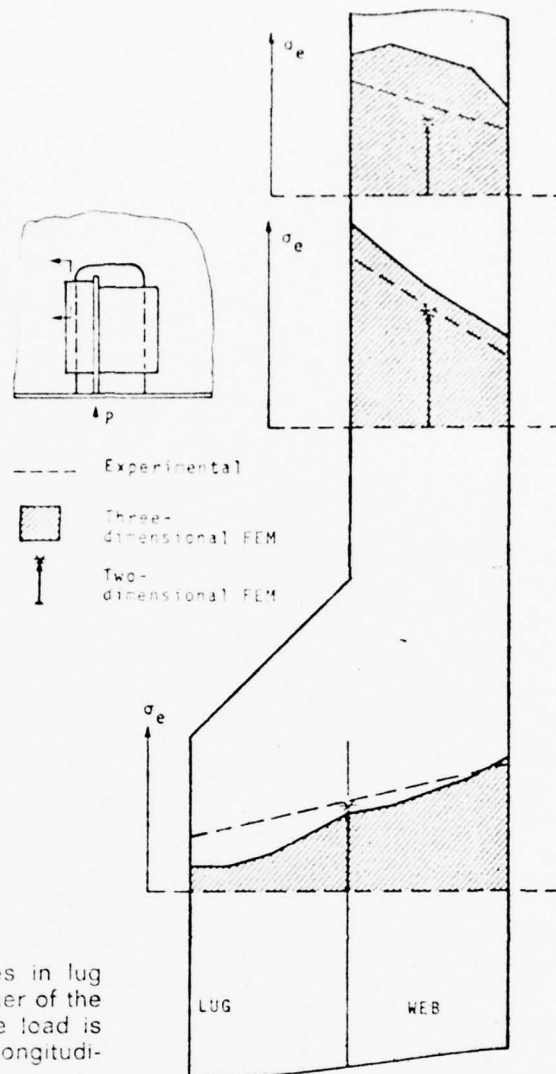
Fig. 16. Equivalent (von Mises) stresses in lug and web close to the upper corner of the lug/web joint, from ref. /8/. The load is applied vertically through the longitudinal.

Results

The conclusions are based on a systematic investigation of various types of connections.

The performance of the connection has been quantified by introducing two stress concentration factors, k_p and k_Q.

k_p represents the stress concentration near the cutout caused by the force P introduced through the longitudinal. k_Q represents a relationsship between the maximum shear stress and the nominal shear stress in the girder caused by the total shear force Q.

The list of symbols is given below. Tables 1–3 contain results in condensed form.

Explanation of tables

The factors k_p and k_Q are not stress concentration factors in the strict sense. But they still contain information about the "stress concentration" for a force P transmitted from the longitudinal and for the girder shear force Q respectively.

$$k_p = \sigma_e / P/_{ht}$$

$$\sigma_e = \sqrt{\sigma_x^2 + \sigma_y^2 - \sigma_x \sigma_y + 3\tau^2}$$

P = the force transferred from longitudinal to the girder

h = the height of the longitudinal

t = the web thickness of the girder

$$k_Q = \tau / Q / H \cdot t$$

τ = the shear stress

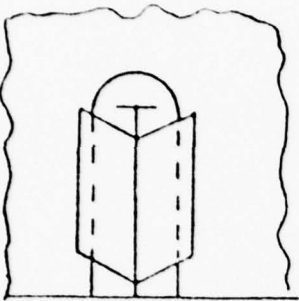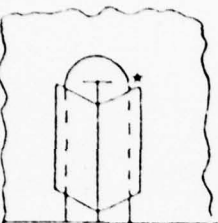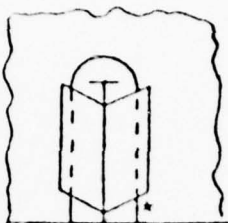Q = the overall shear force

H = the web height of the girder

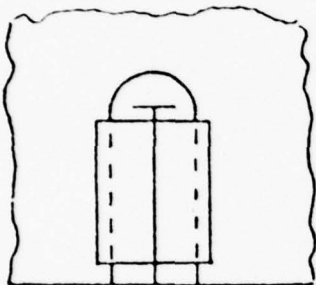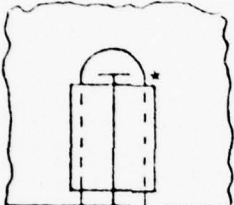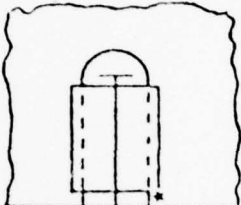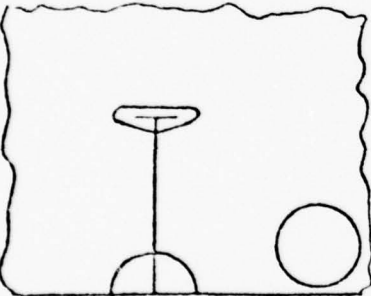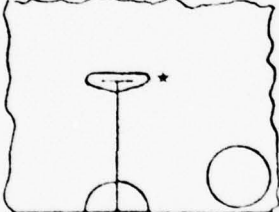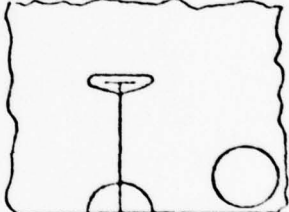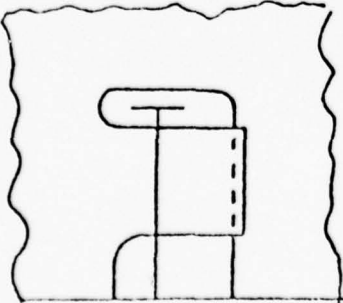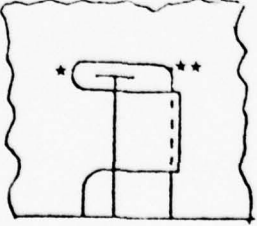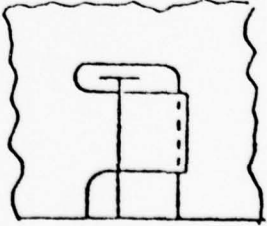s = the web height of the vertical stiffener

P_B = the force transferred through the lug(s)
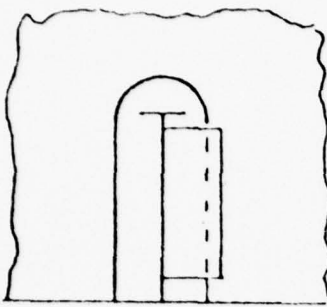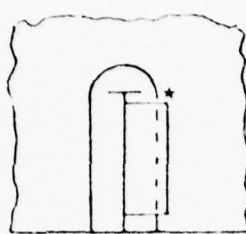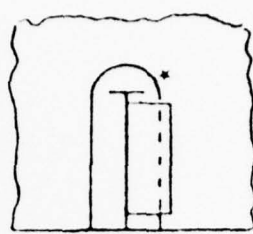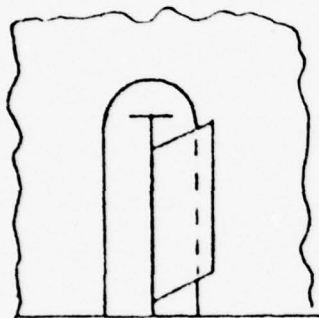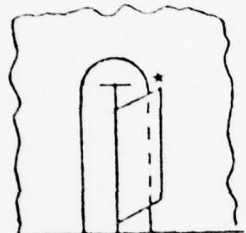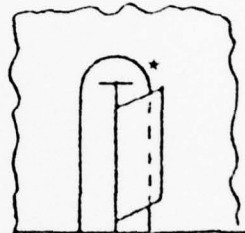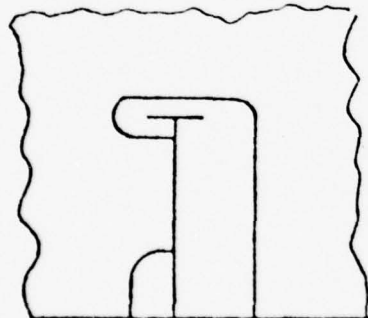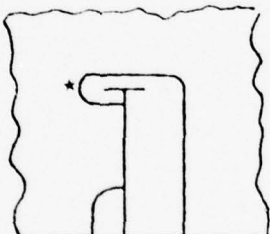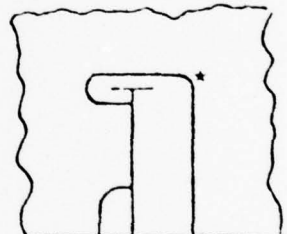
P_T = the force transferred through the vertical stiffener

$\sigma_{e\ all}$ = maximum allowable equivalent stress (Henck von Mises)

21
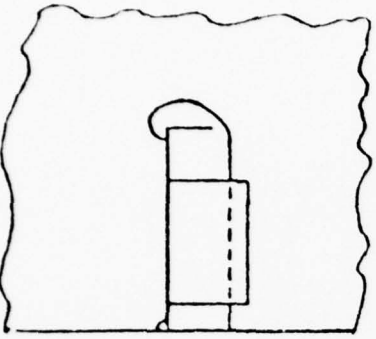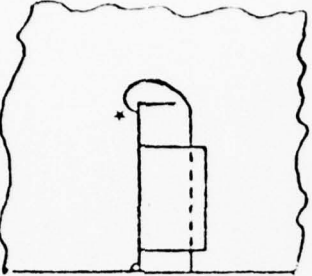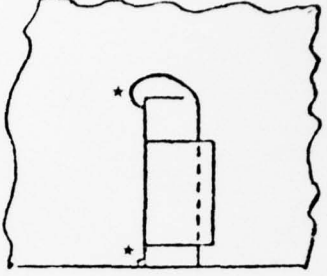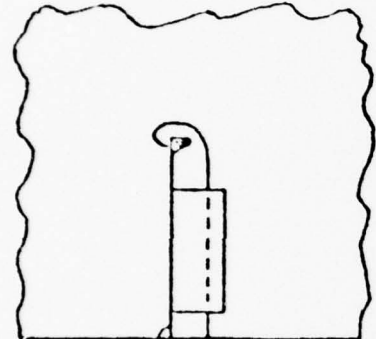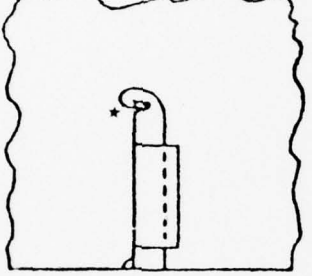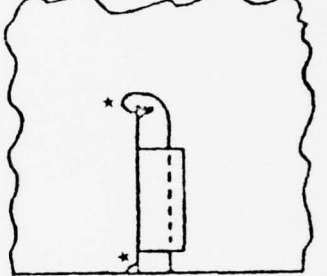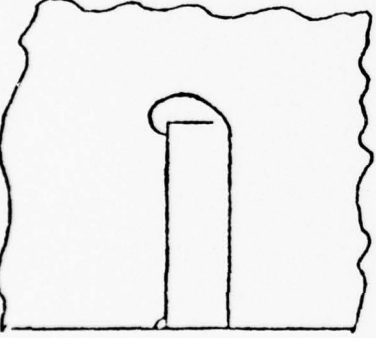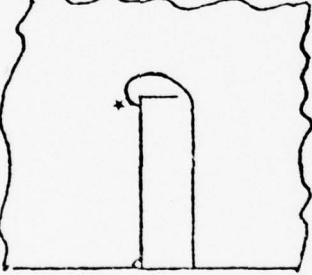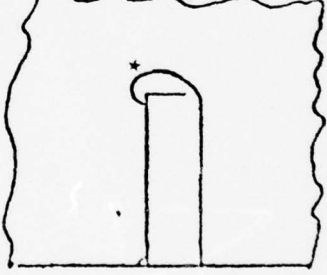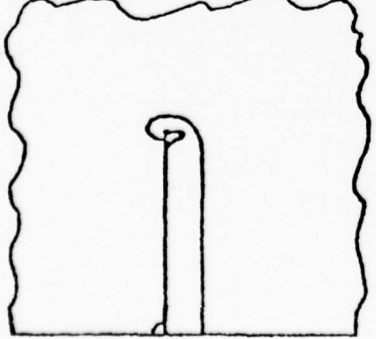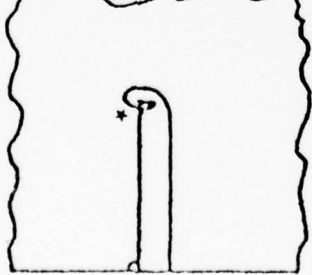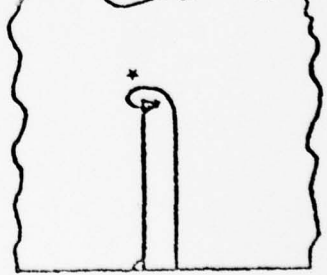
Type	k_p	k_Q
1	$k_p = 1.8$	$k_Q = 1.35$
2	$k_p = 1.8$	$k_Q = 1.35$
3	$k_p = 1.9$	$k_Q = 1.0$
4	★ $k_p = 2.4$ ★★ $k_p = 2.2$	$k_Q = 2.4$

Tab 1

Type	k_p	k_O
	$k_p = 40 \cdot 0$	$k_O = 2.9$
	$k_p = 40$	$k_O = 2.9$
	$k_p = 5.8$	$k_O = 5.2$

Tab. 2

23

Type	k_p	k_Q
	$k_p = 1.8$	$k_Q = 1.3$
	$k_p = 2.2$	$k_Q = 1.3$
	$k_p = 3.6$	$k_Q = 3.1$
	$k_p = 4.8$	$k_Q = 3.1$

Tab. 3

A vertical stiffener connection, fig. 1, may be introduced for two reasons:

i) The lugs alone cannot transfer the force P.
ii) To reduce danger of buckling and vibration of girder.

The size and location of such an element is important. The aim should be a smooth stress distribution in a section parallel to the longitudinal. That is: the force transfer should be as centric as possible with respect to the web plate.

Table 4-7 give results for some different designs of the connection between a longitudinal and vertical stiffener or kneeplate.
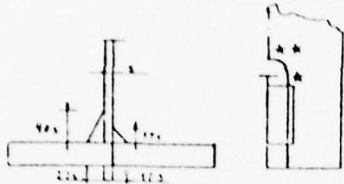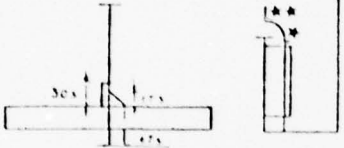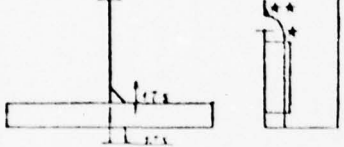
		P_B/P	P_T/P	$\overset{*}{\sigma}_c/P/ht$	$\overset{**}{\sigma}_c/P/ht$	$P_{max}/ht\sigma_{till}$
		0.55	0.45	0.78	1.24	1.16
		0.53	0.47	0.73	0.94	1.58
		0.49	0.51	0.67	0.87	1.7

Tab. 4
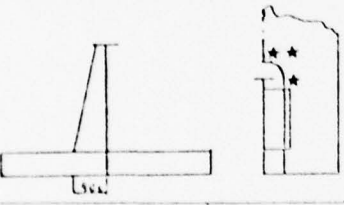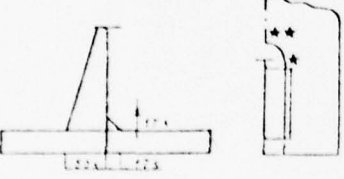
		P_B/P	P_T/P	$\overset{*}{\sigma}_c/P/ht$	$\overset{**}{\sigma}_c/P/ht$	$P_{max}/ht\sigma_{till}$
		0.48	0.52	0.64	0.92	1.6
		0.50	0.50	0.68	0.87	1.7
		0.38	0.62	0.47	0.67	2.22

Tab. 5

		P_B/P	P_I/P	$\sigma_c/P/ht$ *	$\sigma_c/P/ht$ **	$P_{max}/ht\sigma c_{till}$
		0.54	0.46	0.77	1.0	1.5
		0.565	0.435	0.79	1.25	1.18
		0.89	0.11	1.54	0.80	0.96

Tab. 6

		P_B/P	P_I/P	$\sigma_c/P/ht$ *	$\sigma_c/P/ht$ **	$P_{max}/ht\sigma c_{till}$
		0.78	0.22	1.32	0.35	1.12
		0.525	0.475	0.72	1.0	1.48

Tab. 7

Design recommendation

The practical conclusions obtained from this investigation are listed below.

A double-sided lug connection has a maximum stress that is considerably less than half of that in a connection with only one lug.

*   Maximum stress

**   —————— " —————— Twice as large as *

26

A symmetrical design gives a better transfer of forces to the girder, and therefore has smaller stresses than an asymmetrical one.
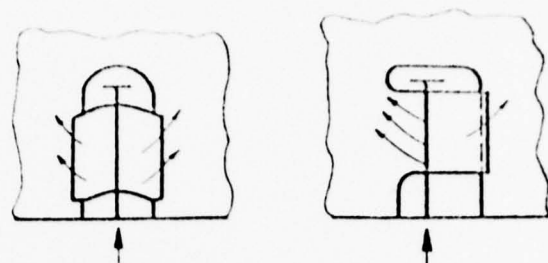
A large cutout breadth results in relatively large bending stresses in the lug near to the longitudinal
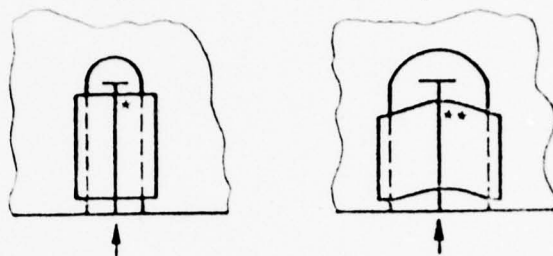
The maximum stresses decrease considerably with increasing height of the lug.
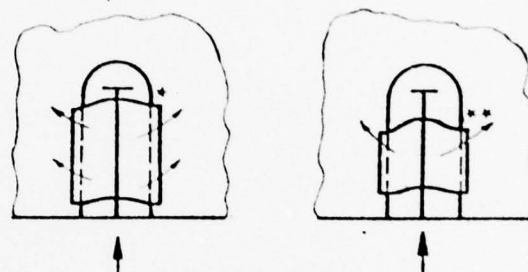
In two-sided lug connections the over all shear force in the girder will cause the highest stresses below the lug fixation point.
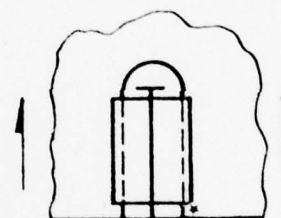
In a one-sided lug connection the maximum stresses will always appear above the lug.
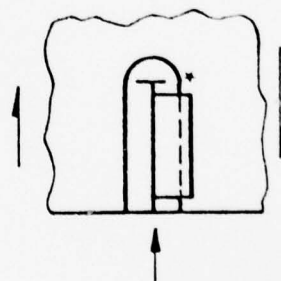
The stress concentration factor is very sensitive to the corner radius in the cutout when the height of the cutout is less than half of web height, fig. 13.
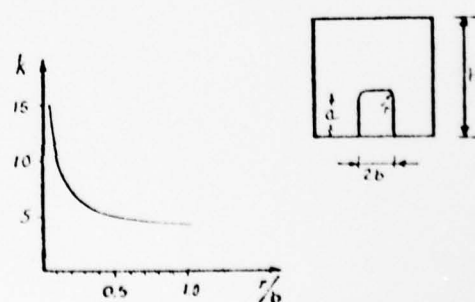
Cutouts in web plating in order to get sufficient throughflow area should preferably be located as separate cutouts between cutouts for longitudinals, and if possible at the middle of the girder span.
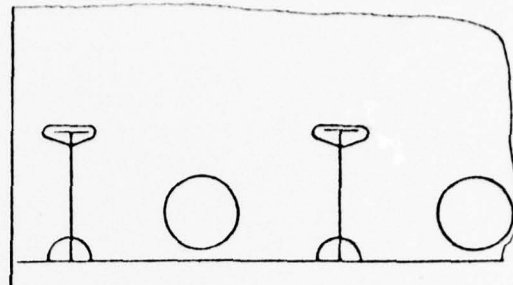
When the force to be transferred from the longitudinal to the girder exceeds the force-carrying capacity of the two lugs alone a common solution has been to locate a vertical stiffener at the web plate and connect this stiffener to the longitudinal. This connection must, however, be very well designed in order to avoid cracks at the weld between the longitudinal and the vertical stiffener.
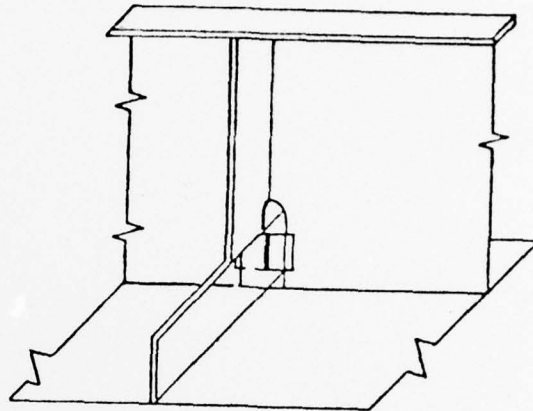
It is important that the vertical force is evenly distributed to the longitudinal i.e. minimum excentricity relative to the web plate.
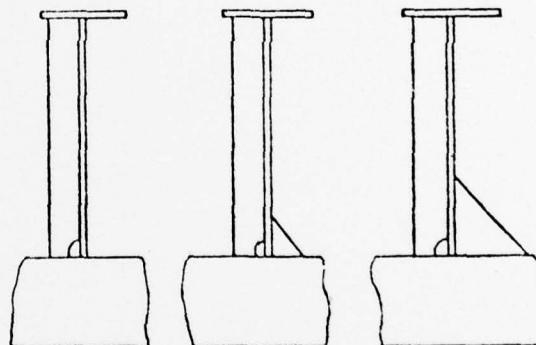
Excentric   Balance   Excentric

If the vertical stiffener is placed there in order to contribute to force transmission only, it may be of moderate length (e.g. 3 times its own height).
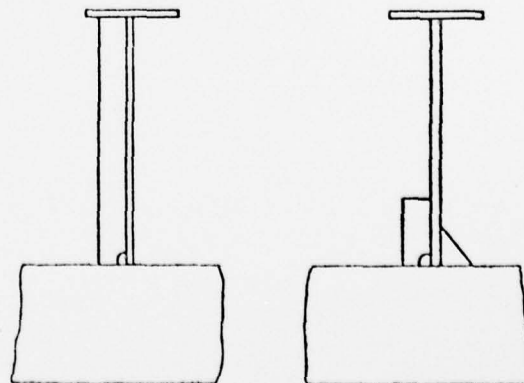
References

1) M. Gibzstein: «Photoelastic investigation of the stress-distribution in the neighbourhood of cut-outs in girders».
DnV report.

2) L. Iversen: «Hårdtværskader, omfang og mulig årsak».
Kursdagene NTH 1972.

3) K. Haslum: «Matrisestatikk og elementmetoder i analyse av skipskonstruksjoner».
Tapir 1974.

4) O. C. Zienkiewics: «The finite element method in engineering science».
Mc Graw Hill 1971.

5) P. Lersbryggen: «Spantgjennomføring».
DnV, August 1972.

6) H. J. Hangen: «Über das Beanspruchungsverhalten des Konstruktionsdetails Längsspantdurch-ten des Konstruktionsdetails Längsspantdurch-

führung und Anschluss an den Rahmensteg bei Tankern».
Schiff und Hafen, Heft 4/1974.

7) Broelman, J. u.a.
Untersuchungen an der Detailkonstruktion Längsspantdurchführung am Tankerrahmen.
Institut für Schiffbau, Universität Hamburg.
April 1975.

8) Berge, S.: «Experimental Stress Analysis of the Longitudinal Girder Connection».
Report R32, Division of Ship Structures, The Norwegian Institute of Technology.

9) K.-J. Bathe, E. L. Wilson, F. E. Peterson, SAP IV — A Structural Analysis Program for Static and Dynamic Response of Linear Systems. Division of Structural Mechanics, The Norwegian Institute of Technology 1973.

Hull responses to hydrodynamic forces on bow flare

by

Sverre Gran, Harald Olsen and Finn Tellsgård,
Research Division, Det norske Veritas

Abstract

A simplified model and procedure is employed to estimate hydrodynamic forces on a bow with large flare, and the resulting vertical bending moment along a ship hull. The dynamic amplification due to hull flexibility is considered and the effect appears to be significant for loads with the predicted magnitude and duration (1.2–2 sec.). It is suggested that the short term distribution of loads and stresses due to bow flare impact can be described by Weibull probability distributions.

The influence of ship speed and sea state on the loads and responses are investigated to some extent, and it is concluded that the influence of ship speed is relatively much stronger at severe sea states.

1. Introduction

Several fast cargo ships have in recent years experienced severe buckling damages in deck (and also bottom) plating, apparently due to unexpectedly high longitudinal stresses /1/. A few measurements on a sister of one seriously damaged ship, /2/, indicated that rather high, but short lasting stress peaks occurred under certain conditions. It was concluded that they related to immersion of the strongly flared bow, a process which has earlier been studied to some extent, e.g. /3/. The hydrodynamic forces created under such immersion have, however, so far been of little concern to the ship designer. The reason for this may be that previous combinations of forebody hull shape, ship speed, hull stiffness etc. have been such that the unfavourable forces and responses were avoided.

With the present paper it is intended to illustrate some of the fundamental features regarding the hydrodynamic loads and corresponding hull respon-

ses created by bow flare immersion. The importance of some design and ship operation parameters will be discussed.

Some of the analytical models that are employed herein are considerably idealized. Hopefully this will provide a better insight into the various aspects of the problem, and it is believed that the most significant features of the involved physical phenomena have been retained.

2. Hydrodynamic forces on flared bow

The commonly used strip theory is based upon linear relationship between the ship motions, the wave surface displacements and the forces acting upon the hull. This assumption is violated when the non-wall-sidedness of the ship's sides becomes pronounced, as in the case of strongly flared sections. Bow flare forces are thus a kind of load where a linear super-

position technique is not applicable. In order to provide an understanding of how the hydrodynamic bow flare forces can be estimated, we shall consider the two-dimensional problem of a solid body penetrating a water surface with an initial high relative velocity V_0. See fig. 1. At a later stage the relative
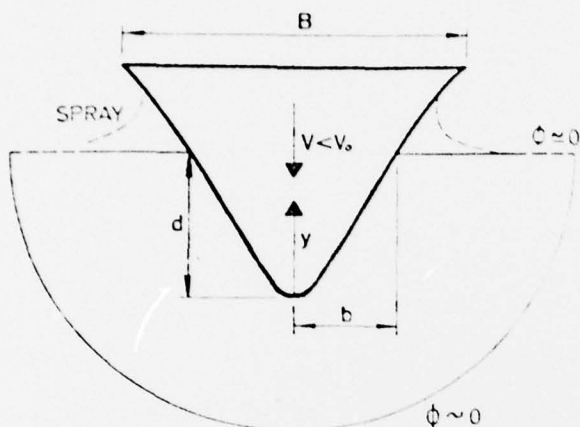
Fig. 1. The simplified two-dimensional problem.

velocity is V such that $V < V_0$, and from the conservation law of momentum the following equation is obtained

$$MV_0 = (M+M')V \qquad (1)$$

where

M = mass of solid body, and
M' = hydrodynamic (or added) mass

and all external forces such as gravity and buoyancy are neglected. As the penetration proceeds, the geometry of the submerged portion of the body changes and M' is therefore not a constant in time. The impact force at any instant is given by

$$F_{imp.} = -M\frac{dV}{dt} = M'\cdot\frac{dV}{dt} + V\frac{dM'}{dt} \qquad (2)$$

which shows that the force is determined by the instanteous value of M' and its time derivative. From this equation it should be evident that a satisfactory method to determine M' is essential.

The penetration of the water surface by a solid body creates a fluid motion throughout the volume of water. If the water is assumed to be incompressible and non-viscous, and the fluid motion to be two-dimensional and initially at rest, this motion is a potential flow described by a velocity potential ϕ.

The kinetic energy of water generated by the solid body may be written:

$$E_{kin} = \frac{1}{2} \iiint\limits_{V} (\nabla\phi)^2 \rho\, dv = \frac{1}{2} \iint\limits_{S} \rho\phi\nabla\phi\cdot nds \qquad (3)$$

where:

ρ = density of fluid
$\nabla\phi$ = velocity of the fluid particle

$(\nabla = i\frac{\delta}{\delta x} + j\frac{\delta}{\delta y}$ in cartesian 2-dimensional coordinates)

v = volume of the part of the fluid bounded by S
S = boundary of the part of the fluid considered
n = outer normal unit vector to the area S

The incompressability of the water and Gauss theorem is made use of when the surface integral is obtained. The area of integration, fig. 1, consists of the free water surface, the wetted part of the solid body and a semicircle of infinite radius. Along the semicircle and the free water surface it is assumed that $\phi = 0$. The last simplification implies that the effect of piled-up water (spray) is not taken into account.

The definition of the added mass from kinetic energy considerations is given by:

$$M' = \frac{E_{kin}}{\frac{1}{2}V^2} = \frac{1}{V^2} \iint\limits_{S} \rho\,\phi\nabla\phi\cdot nds \qquad (4)$$

where S is reduced to the wetted part of the solid body. This defines a well known mathematical problem but has nevertheless an analytical solution for a very small number of cases. One of these cases is the solid body shaped as a circular cylinder, and by means of conformal mapping this special solution may be applied to a variety of different forms.

The immersion of the solid body will continuously change the added mass and it is therefore important to underline that this approach is based upon a quasi-stationary consideration, i.e. the water flow at each instant is taken to be identical with steady state flow.

A computer program which calculates impact forces on a ship's forebody is developed and the method used is the same as outlined above. The conformal mapping made use of in the program is a two-parameter version called Lewis' transformations /4/ which is especially efficient to transform a circle to shiplike sections.
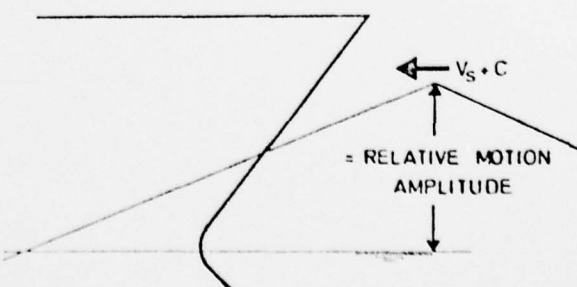
Fig. 2. Simple bow/wave model.

In order to compensate for the effect of piled-up water, a correction based on the theoretical treatment of the wedge impact problem /5/ is included in the computer program.

2.1 Deterministic Load Model

For application to the ship's forebody the computations are based upon the following idea:

A reference system is fixed to the hull.

Only head waves are considered and from this reference system each station along the bow will feel a «wave» passing with a velocity equal to the sum of the ship speed V_S and the actual wave celerity, C, see fig. 2 above. The amplitude of the «wave» will in general not be the surface wave amplitude but rather the vertical relative motion RM incorporating the heave and pitch motions of the bow.

For practical purposes we shall in the following employ the vertical relative motion at the forward perpendicular. This implies that the variation of the relative motion amplitude along the forebody is disregarded. For further simplification this «relative motion wave» is approximated by a «triangular wave».

A consequence of this approximation is that the vertical relative velocity is a constant in time proportional to the corresponding vertical relative motion, and this implies that the vertical relative velocity is overestimated during the later stage of the bow immersion process when the transfer of momentum between ship and sea has become large enough to cause a reduction in this velocity.

When the «triangle wave» propagates along the hull it may give rise to hydrodynamic loads on the bow. These loads are estimated by means of a kind of strip theory. The ship's forebody is divided into strips which are all parallel and tried to be so arranged that the «step effect» is minimized. (This «step effect» is a three-dimensional effect which results from inevitable discontinuities at the junction between two-dimensional strips). In this paper the vertical impact forces are required and the strips are therefore taken to be vertical, see fig. 3. The bow

impact force and average pressure are calculated for each strip by means of the method described in the previous paragraph. The forces are then summed to give the resultant vertical load on the forebody at a specified number of points in time. Finally, the amplitude and duration of the load are estimated when this is approximated with a half-sine function, which is a convenient form for the purpose of calculating the resulting stresses (Appendix A). This results in a force of short duration (approx. 1.2–2 sec.) and of significant magnitude in most conditions.

In the previous paragraph the non-linear feature of the hydrodynamic loads due to bow flare was mentioned. We now assume that the hydrodynamic impulse, beyond that obtained by linear theory, is such that its effect upon the ship motions is negligible. This implies that relative motions as found by linear theory are applied in conjunction with the above impact theory.

This assumption combined with the «triangle wave» approximation leads to a probable overprediction of the loads in accordance with model tests to which results from our computer program have been compared.

2.2 An idealized stochastic description of loads in random head waves

As described in the preceding section, the hydrodynamic force imposed upon a strip is governed by the vertical relative motion and the vertical relative velocity. In a stationary state of (irregular) waves, the time functions of these two are random variables which can be defined by a variance vs. frequency (ω_e) spectrum, fig. 4, and *their single amplitudes*
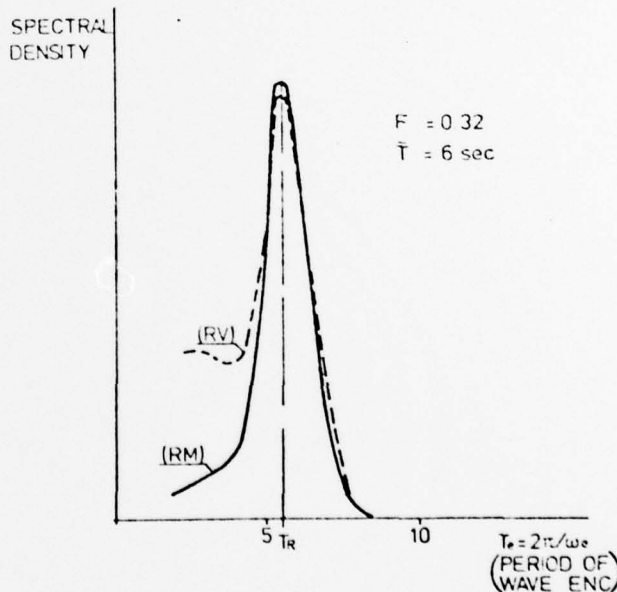
Fig. 4. Response spectra for relative motion and velocity.

Fig. 3. Division of a ship's forebody into vertical strips.

$\overline{RM}$ and $\overline{RV}$ have a probability of exceedance described by the well-known Rayleigh distribution. For $\overline{RM}$ this distribution reads:

$$Q(RM \geq r) = \exp\left(-\frac{r^2}{E_{RM}}\right) \qquad (5)$$

$$\overline{RM} = \frac{T_R}{4} \cdot \overline{RV} \qquad (6)$$

where:

$Q(RM \geq r)$ is the probability that RM shall exceed the value r.

E_{RM} is half the variance of the time signal $RM(t)$, i.e. half the area under the response spectrum for $RM(t)$.

We consider now for simplicity incoming waves from ahead only, producing time variations of relative motion and velocity which are idealized as follows:

—The time variation of the idealized relative motion consists of triangular cycles with a unique period. This period is taken to be equal to the period of encounter T_R which corresponds to the peak of the relative motion response spectrum, see fig. 4.

—The time variation of the idealized relative velocity is periodic with the same period T_R as the relative motion. (Justification of this assumption is obtained by considering actual response spectra).

—The amplitudes $\overline{RM}$ and $\overline{RV}$ as idealized follow the Rayleigh distribution for the actual $\overline{RM}$ and $\overline{RV}$ peaks, eq. 5.

The simplification that $\overline{RM}$ and $\overline{RV}$ have equal periods, which are also invariant in a given sea state, leads to a fixed relationship between corresponding pairs of amplitudes $\overline{RM}$ and $\overline{RV}$:

Employing the method explained in paragraph 2.1 the vertical bow force $F_{V,i}$ corresponding to a given pair (RM_i, RV_i) can be calculated. Since this force will increase monotonously with increasing $\overline{RM}$ (and $\overline{RV}$), it is readily deduced that the probability of exceedance for the bow force is:

$$Q(F_{V,i}) = Q(\overline{RM_i}) = Q(\overline{RV_i}) \qquad (7)$$

This relationship provides a possibility to establish the probability distribution of F_V as follows:

For several levels of bow immersion, i.e. for several values of RM, the corresponding magnitude of F_V is computed. The probability for exceeding the individual levels of $\overline{RM}$ is obtained from eq. (5), which in view of eq. (7) yields the probability for exceeding the corresponding forces F_V.

3. Hull responses to bow flare forces

The hydrodynamic force acting on the hull entrance will cause an acceleration of the ship and a distribution of bending moments along the hull. The simplest approach is to consider the hull as rigid and with uniform mass distribution. However, experience has shown that impulsive forces of the present nature are often accompanied by hull vibration. The somewhat more complicated approach taking hull deformations into account may therefore sometimes be required. The present section presents some

Fig. 5. Elucidation of the procedure employed to derive the bow force probability distribution.

alternative ways of estimating the bending moments and accelerations.

3.1 Rigid, uniform hull

If the ship is considered perfectly rigid, the heave and pitch motion caused by the vertical bow force will be determined by

$$(M + M') \ddot{Z}(0) = F_v \tag{8}$$

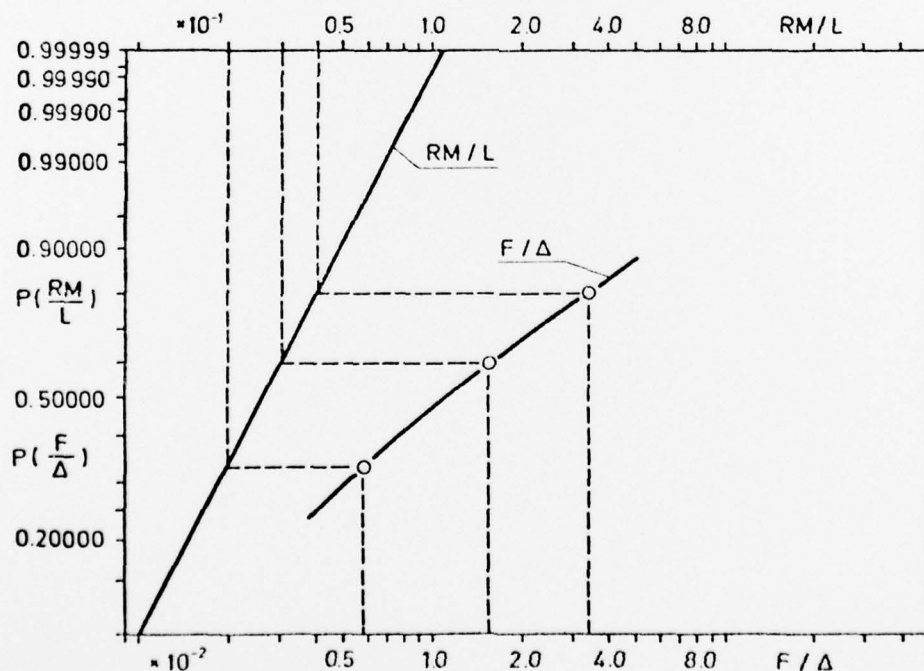$$I \ddot{\phi} = F_v \, L/2 \tag{9}$$

where

M = ship mass
M' = added mass of water
$\ddot{Z}$ = vertical acceleration at centre of gravity supposed to be located amidships

F_v = vertical bow force, function of time
I = vertical moment of inertia of the ship and added mass of water = $(M + M') L^2/12$
$\ddot{\phi}$ = pitch acceleration
L = ship length

The vertical acceleration at a distance x from amidships during the force action is

$$\ddot{Z}(x) = \ddot{Z}(0) + x \ddot{\phi} = (1 + 6x/L) F_v/(M + M') \tag{10}$$

The bending moment at a point x' is founded by summing up the moment contributions from the bow force and the forces of inertia from the bow to the point x'.

$$M_v(x') = (L/2 - x') F - \int_{x'}^{L/2} m \ddot{Z}(x) (x - x') \, dx \tag{11}$$

$M_v(x')$ = vertical bending moment at x = x'
m = ship and fluid mass per unit length = (M + M')/L

Introducing (10) in (11) gives the bending moment

$$M_v(\xi) = \frac{1}{8} (1 + 2\xi - 4\xi^2 - 8\xi^3) F_v L \tag{12}$$

where $\xi = x'/L$. A plot of the function $M(\xi)/FL$ is given in Fig. A1 as the curve obtained for the hull with infinite natural frequency.

Maximum bending moment is:

$$M_{v, \max} = 0.148 \, F_v L \text{ for } \xi = x/L = 0.167 \tag{13}$$

The buoyancy forces and the corresponding acceleration component do not contribute to the bending moment when the ship is approximately uniform.

3.2 Flexible hull

The bending moment of the ship induced by bow flare forces may also be studied in terms of normal modes. This method covers the rigid hull case by letting the natural frequencies approach infinity, but offers also the possibility to study the effect of flexibility on the bending moments.

The vertical motion of the ship may in general be written

$$Z(\xi, t) = \sum q_i(t) \psi_i(\xi) \tag{14}$$

The mode shape functions ψ_i are chosen to be dimensionless and with unit value in the bow. The coordinate q_i therefore describes the bow displacement in metres.

The index i can be chosen as the number of nodes of the mode. i = 0 and i = 1 thus describe the heave and pitch modes respectively. However, since the bending moment will now be deduced from the deformations, these two modes may be omitted, because they do not contribute to the deformation. The summation will thus be taken over i = 2, 3, 4, ··· N, corresponding to the 2 node, 3 node ··· N node modes.

The deformation of the ship is described by the differential equations of the normal coordinates.

$$\ddot{q}_i + 2a_i \dot{q}_i + \omega_i^2 q_i = F_v(t)/\Gamma_i \tag{15}$$

where

a_i = damping factor of mode i
ω_i = circular natural frequency of mode i
Γ_i = inertia coefficient of mode i.

When the bow force and ship deformation is zero up to time t = 0, which may always be realized, a general solution of this equation is the convolution integral

$$q_i(t) = \frac{1}{\omega_i \Gamma_i} \int_0^t e^{-a_i(t-\tau)} \sin \omega_i(t-\tau) F_v(\tau) \, d\tau \tag{16}$$

Now the vertical bending moment of the hull at a location $x = \xi L$ is expressed by the normal mode representation through

$$M_v(\xi, t) = EI \, L^2 \frac{\partial^2 Z(\xi, t)}{\partial \xi^2} \tag{17}$$

$$= \sum_{i=2}^{N} \frac{EI L^2}{\omega_i \Gamma_i} \frac{\partial^2 \psi_i(\xi)}{\partial \xi^2} \int_0^t e^{-a_i(t-\tau)} \sin \omega_i(t-\tau) F_v(\tau) \, d\tau$$

where EI is the vertical bending stiffness module at the location $x = \xi L$. This expression is valid for an arbitrary vertical bow force process and also for an arbitrary distribution of mass and elasticity along the hull. One has to determine the shape of the natural modes, the natural frequencies and mass coefficients, which is a standard problem with many tools for solution. In addition one has to find relevant values for the damping coefficients in the cases when the solution is sensitive to damping.

3.3 Flexible uniform hull, semisinusoidal force

In order to study the influence of flexibility, damp-

33
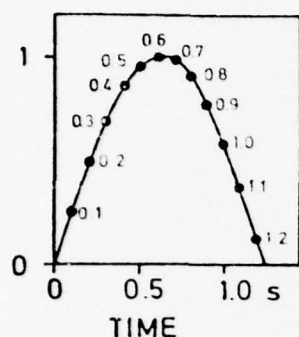
b) INSTANTANEOUS BENDING MOMENT
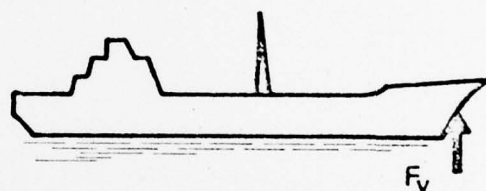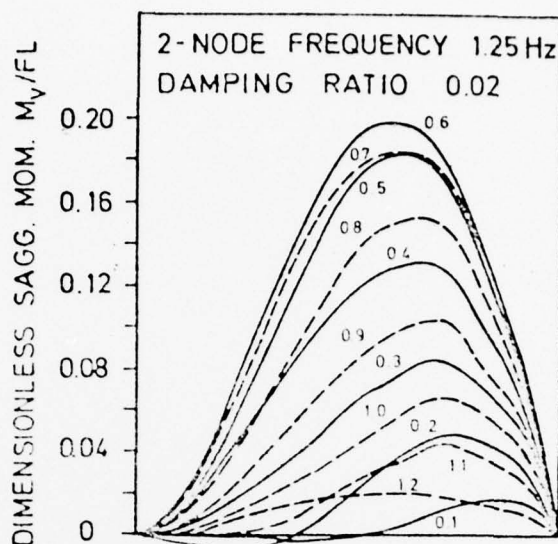
a) FORCE CYCLE

Fig. 6 A semisinusoidal force of duration 1.25s is
shown in a). In b) is displayed the bending
moment profile along the hull at different
times during the force cycle.
(Uniform hull).

ing etc. on bow flare forces, it is convenient to
investigate a particular ship/force model where the
bending moment is obtained as an analytic expres-
sion.

For this purpose a uniform ship will be studied.
Uniform ships have been thoroughly investigated by
previous authors, for instance by Bishop et.al. /6, 7/.

The derivation of the bending moment in this case
is given in Appendix A.

Among other parameters, the bending moment
induced by the bow flare force will depend on the
flexibility of the hull and the damping of the normal
vibrations. As a measure of flexibility or stiffness,
we may use the natural frequency of the 2-node
mode vibration, $f_2 = \omega_2/2\pi$. As a measure of damp-
ing, the damping ratio $\lambda = a/\omega$ will be used, and this
quantity will be assumed equal for all modes.

For this part of the investigation a real case will
be considered where the main parameter values are:

Duration of bow force	1.25 s
Two node mode natural period	0.8 s
Two node mode frequency	1.25 HZ
Damping ratio	0.02

The bending moment is given dimensionless with
respect to (force amplitude x ship length).

The distribution of bending moment along the hull
during the force cycle is displayed in fig. 6. It is
observed that the bending moment contains an im-
pulse component which propagates backwards along
the hull during the force action. The maximum bend-
ing moment is seen approximately to coincide with

the maximum force. The largest bending moment
value is 0.198 and is experienced at about $\xi = 0.1$.
These values correspond to a bending moment of
0.148 at $\xi = 0.167$ in (13) which was derived for a
perfectly rigid hull. It is thus seen that the flexibi-
lity gives an amplification of 34 % of the maximum
bending moment in this case.

To study a rather more closely how response depends
on rigidity, the midship bending moment is plotted
against the 2-node frequency in fig. 7. It is observed
that for the present force the influence would be
negligible at a natural frequency of 2 Hz. This result
indicates the rule that if a bow force has shorter
duration than 2½ natural 2-node periods, the flexi-
bility should be taken into account.

The response curve in fig. 7 is indicated for some
alternative values of the damping ratio. The actual
values of the damping ratio for real ships are known
to lie between 0 and 0.05. See for instance /8/. In this
range it is concluded from the figure that the bend-
ing moment is only slightly dependent on the damp-
ing.

To investigate the transient vibrations induced by
the bow force, fig. 8 has been prepared. This figure
shows the midship bending moment induced by the
bow flare force of duration 1.25 s. It appears that
the amplitude of the transient vibration is only
about 1/10 of the response within the force action
period. In this respect the bow forces studied here
are of a quite different nature from the slamming
force and whipping response.
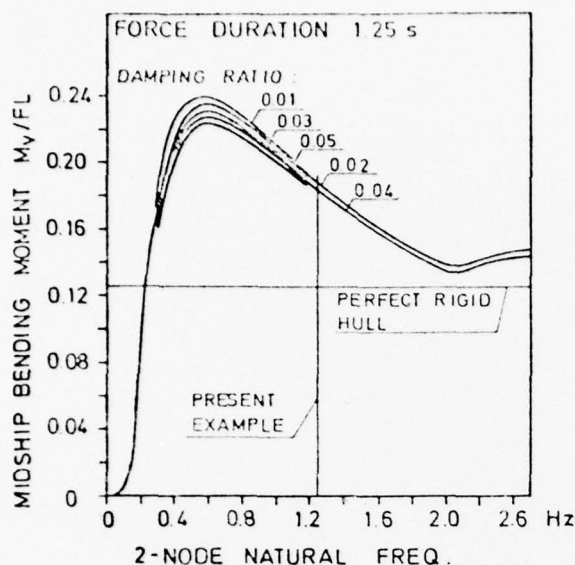
Fig. 7. Variation of maximum midship bending moment with the 2-node natural frequency and damping ratio. (Uniform hull).
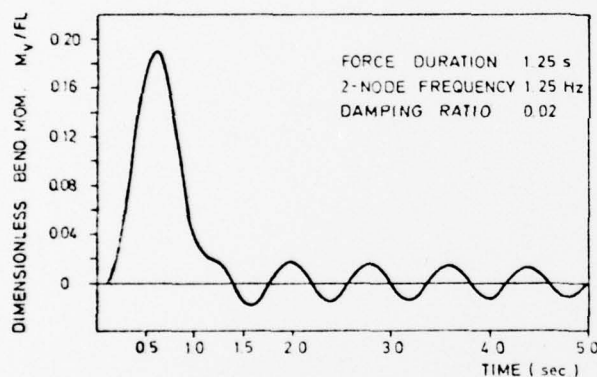
Fig. 8. Time variation of midship bending moment.

Fig. 9. Body plan of the actual ship.

MAIN SHIP DATA	
Length between perpendiculars	165 m
Draught (even keel)	8.1 m
Beam	23.6 m
Displacement (Δ)	23000 tons

Table 1.

4. Application to fast cargo ship in various sea states

The previously mentioned computer program has been employed to calculate loads and bending moments on a ship which was seriously damaged some years ago. One of the most striking qualities of the ship is the small stem angle ($\sim 47.5°$) giving rise to tremendous vertical impact forces. The ship had further an extreme bow flare and a relatively high maximum speed (~ 21 knots).

Fig. 9 shows the body plan and table 1 gives the relevant ship data.

The main objective of this application is not to present quantitatively reliable results for this particular ship, but to indicate how various parameters such as sea state and ship speed may influence the resulting wave-induced bending moments and stresses, and how these moments and stresses vary along the hull. The influence of bow flare shape is not considered but an indication of the importance of this feature is given in appendix B.

The foremost quarter length of the ship was divided into 11 vertical strips of equal length.

The relation between vertical relative motion $\overline{RM}$ and vertical relative velocity $\overline{RV}$ for «triangular waves» was given in eq. 6. These relations were determined for five conditions consisting of two ship speeds combined with three sea states by means of a comparison of the response spectra of $\overline{RM}$ and $\overline{RV}$. The wave period corresponding to the common peak value T_R was then used in eq. 6 (see fig. 4).

Between 5 and 12 values of $\overline{RM}$ (and $\overline{RV}$) were used as input to the computer program, each value of $\overline{RM}$ giving one value of vertical impact force F_V for constant ship speed and sea state.

4.1 Calculated longitudinal stresses in deck

Three sea states were selected to demonstrate the

influence of different wave heights and wave periods on this kind of loads and responses.

These sea states were chosen from three reasonable values of significant wave height $H_{1/3}$ subject to the condition that the characteristic wave steepness number s should be 1/20, where

$$s = \frac{H_{1/3}}{\frac{g}{2\pi}\overline{T}^2} \tag{18}$$

Two ship speeds were considered, the highest one corresponding to about 20 % above the maximum speed of the actual ship.

The different conditions are specified and listed in table 2.

SEA STATE AND SHIP SPEED			
CONDITION No.	$H_{1/3}/L$	$\overline{T}\sqrt{g/L}$	F_n
1	.018	1.5	.19
2	.018	1.5	.32
3	.036	2.2	.19
4	.036	2.2	.32
5	.055	2.7	.19

Table 2. Considered conditions of ship speed and sea state.

Note that max. ship speed is omitted for the worst sea state, since it would represent a too unrealistic case.

The maximum values of the bending moments along the hull as given in eq. 17 are shown in fig. 10 for the five conditions. The values given are the most probable largest values in a time period of about 1 hour. In order to indicate the variation of

Fig. 11. Probability distribution of vertical bending moment at about L/3 aft of F.P.

the bending moment for different probability levels fig. 11 is prepared, where the method of least squares is employed to fit the computed values to straight lines.

On the basis of the calculated bending moments and actual sectional moduli the bending stress distribution in deck was computed and the results are given in figs. 12 and 13. Again the probability level used corresponds to one exceedance per hour.

Fig. 12 reveals that maximum stresses should occur between L 8 and L/4 from F.P., which is in agreement with the damage picture of the actual ship. It also indicates that the computed stress level, althoug this should be considered only as an order of magnitude, is rather high.

Actually, it is several times higher than the ordinary wave bending stresses in the considered sea states; and it might be high enough to produce buckling and even yielding of longitudinal strength elements in the deck.
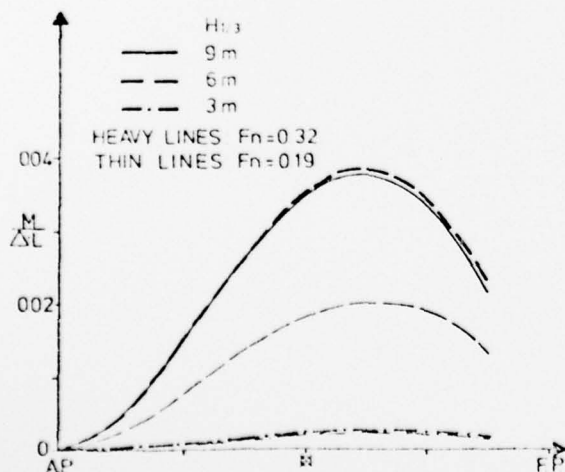

Fig 10. Most probable largest bending moment amplitudes during one hour, at different positions along the hull.

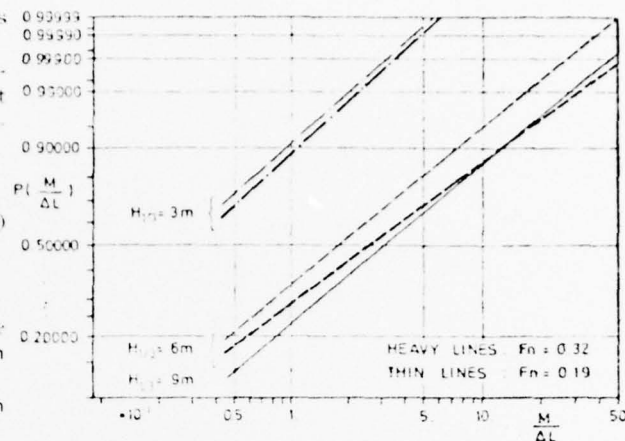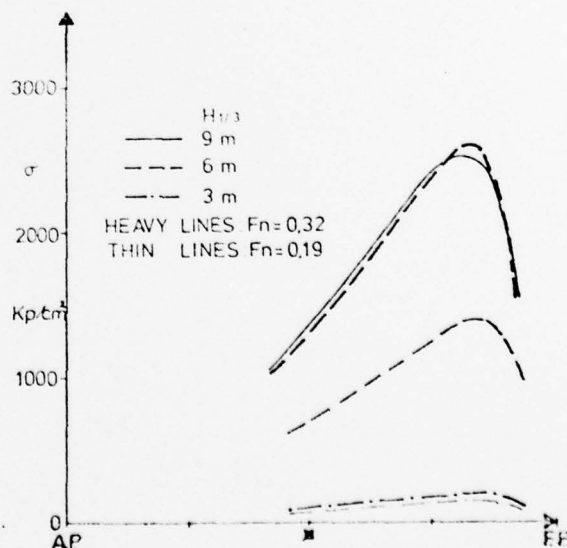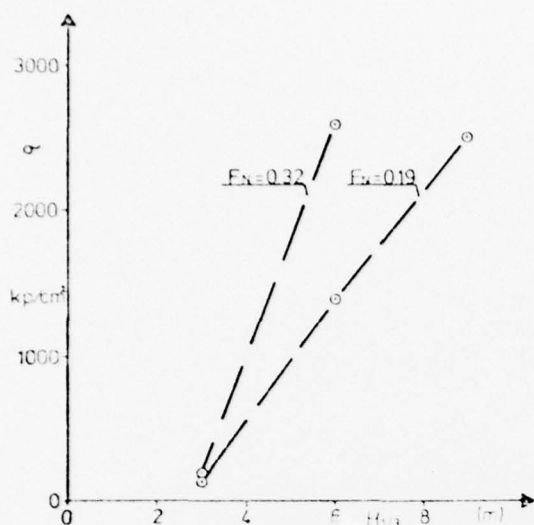Fig. 12. Most probable largest longitudinal stress in deck during one hour.

Fig. 13. Most probable largest longtitudinal stress in deck (during one hour) at L/6 aft of F.P. (where $\sigma \simeq \sigma_{max}$). Influence of sea state and ship speed.

4.2 Influence of ship speed and sea state

It should be evident that the ship speed strongly affects the bow impact forces and associated stresses. Maximum amplitudes of stress in deck for the two ship speeds are therefore shown in fig. 13 as a function of significant wave height $H_{1/3}$.

The effect of a speed reduction under heavy sea conditions in order to prevent high stresses in deck is considerable.

Fig. 13 also shows that for a given ship speed the stresses will increase progressively with increasing significant wave height. At $H_{1/3} < 3$ m the stresses are relatively moderate. This nonlinear behaviour is easily understood in view of the strong influence of bow flare slope ($\frac{db}{dy}$ which increases with distance from the waterplane) and the relative velocity ($F \propto RV^2 \propto H_{1/3}^2$), as discussed in Appendix B.

4.3 Nature of statistical short term distribution of stresses produced by bow impacts

By means of the method of least squares a straight line was fitted to the calculated bending moments of each condition on the Weibull prob. paper. This resulted in a fairly good approximation (fig. 14) and the results may therefore be expressed by means of a Weibull distribution, i.e.

$$Q(M_V \geqslant X) \doteq \exp\left(-(X/A)^m\right) \qquad (19)$$

where the parameters A and m are displayed in Table 3 for the various conditions.

When these parameters are determined it is possible to estimate the most probable largest bending moment during N responses by setting $Q = 1/N$ and thus obtain:
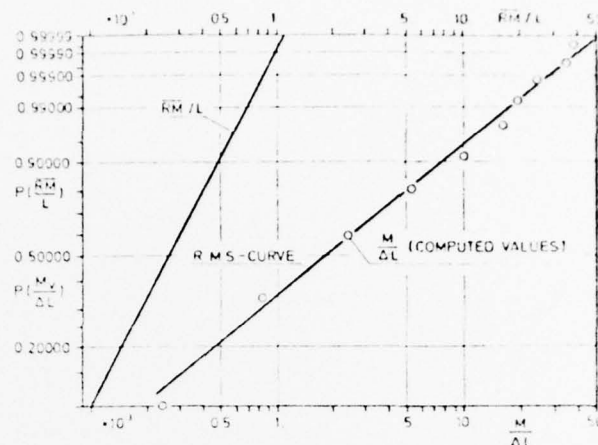
Fig. 14. The fitted straight line compared to the computed values.

COND. NO.	A	m
1	0.00037	0.90
2	0.00044	0.94
3	0.0027	0.85
4	0.0042	0.77
5	0.0048	0.86

Table 3. Parameters of Weibull distribution fitted to computed short term distributions of bending moment.

$$M_{V, max} = A(\ln N)^{1/m} \qquad (20)$$

This equation is valid provided that the sea state may be considered as a stationary wave system, i.e. as long as the short term parameters A and m are constant.

It will be noticed that the exponent m is found to be ~ 0.85 on the average, while $m = 1.0$ would give an exponential distribution. This appears reasonable, since a direct proportionality between the bow impact force (F_V) and RV^2 would, since RV is Rayleigh-distributed, result in an exponential distribution for F_V.

5. Conclusions

(i) Both full-scale measurements and calculations indicate that stresses due to bow flare impact can attain considerable magnitude in the entire forebody. Maximum stress occurs about L/6 aft of fwd. perpendicular.

(ii) Hull flexibility must be included for proper evaluation of stress responses to bow flare forces. Calculations show that a dynamic amplification takes place when the force duration matches the natural periods of the hull.

(iii) Increasing wave steepness, ship speed and vertical relative velocity at bow will tend to increase the stress responses strongly. The in-

fluence of ship speed is relatively much stronger at severe sea states.

(iv) The bow flare impact force increases approximately in proportion to the slope of the ship's side (slope of flare).

(v) It appears that the short term distribution of loads and stresses due to bow flare impact can reasonably well be described by Weibull probability distributions.

Appendix A: Response of uniform, flexible hull exposed to semisinusoidal force

In the case of a uniform, flexible hull, the deformation modes are the same as for transversal vibrations of a slender, uniform bar free at both ends, viz.

$$\psi_i(x) = \begin{cases} \dfrac{\cos\beta_i x}{2\cos\beta_i L/2} + \dfrac{\cosh\beta_i x}{2\cosh\beta_i L/2} & i = 2, 4, 6 \cdots \\[2mm] \dfrac{\sin\beta_i x}{2\sin\beta_i L/2} + \dfrac{\sinh\beta_i x}{2\sin\beta_i L/2} & i = 3, 5, 7 \cdots \end{cases} \quad (A.1)$$

$$\beta_i \cong \frac{\pi}{2L}(2i-1) \quad i = 2, 3, 4, \cdots$$

Neglecting the buoyancy contribution to the restoring forces, one obtains the eigen frequencies as

$$\omega_i^2 = EI \, L \, \beta_i^4 / (M+M') \quad (A.2)$$

where $(M+M')$ is the total mass of the ship and added mass of water.

The inertia coefficients T_i are

$$T_i = (M+M') \int \psi_i(\xi) \, d\xi$$

$$= \begin{cases} (M+M')\left[\dfrac{1}{\cos^2\beta_i L/2} + \dfrac{1}{\cosh^2\beta_i L/2}\right] & i = 2, 4, 6 \cdots \\[3mm] (M+M')\left[\dfrac{1}{\sin^2\beta_i L/2} - \dfrac{1}{\sinh^2\beta L/2}\right] & i = 3, 5, 7 \cdots \end{cases} \quad (A.3)$$

which is approximately equal to $(M+M')/4$ for all modes.

As a bow force convenient for the analytic study, a semisinusoidal force is chosen, viz.

$$F_v(t) = \begin{cases} F_v \sin \Omega t & 0 < t < t_f = \pi/\Omega \\ 0 & \text{otherwise} \end{cases} \quad (A.4)$$

The force is displayed in fig. 6a.

A similar force applied to piano string excitation has been used by Lord Rayleigh /9/.

When the expressions (A.1) through (A.4) are introduced into (17) and the integral is solved, one arrives at the bending moment on the dimensionless form:

$$\frac{M_v}{FL} = \sum_{i=2}^{n} g_i(\xi) \frac{\omega_i^2}{D_i^2} F_i(t) \quad (A.5)$$

In this expression the quantities D_i^2 in the dominators are the impendance-like expressions

$$D_i^2 = a_i^4 + 2a_i^2(\omega_i^2 + \Omega^2) + (\omega_i^2 - \Omega^2)^2 \quad (A.6)$$

Here the two first terms are mainly determined by the damping which is in general small. The last term thus indicates that the bow impact force may give rise to very large bending moments if the force duration matches one of the natural half-periods.

The time dependent functions $F_i(t)$ in (A.5) are defined in the time interval when the force is acting, as

$$F_i(t) = (\omega_i^2 - \Omega^2 + a_i^2)\sin\Omega t - 2a_i\Omega\cos\Omega t$$
$$\qquad (A.7)$$
$$- e^{-a_i t}\frac{\Omega}{\omega_i}\left[(\omega_i^2 - \Omega^2 - a_i^2)\sin\omega_i t - 2a_i\omega_i\cos\omega_i t\right]$$

$$0 \le t \le \pi/\Omega$$

This expression shows that the bending moment consists of one contribution (the two first terms) which follows the bow force with a certain time lag, and one contribution made up of transient, natural vibrations.

In the time after the force has disappeared, the time function is

$$\qquad\qquad (A.8)$$
$$F_i(t) = e^{-a_i t}\left[2a_i\Omega(e^{\pi a_i/\Omega}\cos(\omega_i t - \pi\omega_i/\Omega) + \cos\omega_i t)\right.$$
$$\left. - (\omega_i^2 - \Omega^2 - a_i^2)\frac{\Omega}{\omega_i}(e^{\pi a_i/\Omega}\sin(\omega_i t - \pi\omega_i/\Omega) + \sin\omega_i t)\right]$$

$$\pi/\Omega < t < \infty$$

which is only a sequence of natural vibrations.

The position dependent functions $g_i(\xi)$ in (A.5) are defined as

$$g_i(\xi) = \frac{M+M'}{\beta_i^2 \, T_i}\begin{cases} \dfrac{\cosh\beta_i L\xi}{\cosh\beta_i L/2} - \dfrac{\cos\beta_i L\xi}{\cos\beta_i L/2} & i = 2, 4, 6 \cdots \\[3mm] \dfrac{\sinh\beta_i L\xi}{\sinh\beta_i L/2} - \dfrac{\sin\beta_i L\xi}{\sin\beta_i L/2} & i = 3, 5, 7 \cdots \end{cases} \quad (A.9)$$

These functions have the property that their sum converges towards the bending moment distribution for a rigid bar obtained in (3.5), that is

$$\sum_{i=2}^{\infty} g_i(\xi) = \frac{1}{8}(1 + 2\xi - 4\xi^2 - 8\xi^3) \quad (A.10)$$

This can be concluded from the fact that perfect rigidity is obtained by letting the eigen frequencies ω_i approach infinity in the equations (A.5) through (A.8) which leads to (A.10).

Appendix B: A simple model for investigation of blow flare effects

With reference to § 2 the conservation of momentum principle implies that

$$M V_0 = (M+M')V \quad (B1)$$
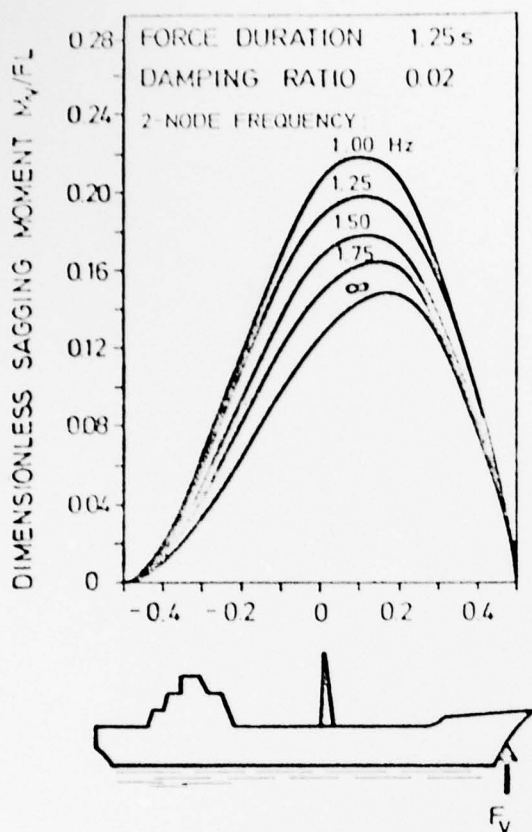
such that the bow impact force F_{imp} may be written

Fig A1. Variation of the maximum bending moment profile with hull flexibility. (Uniform hull)

$$F_{imp.} = -\dot{M} \cdot V = M' \frac{dV}{dt} + V \frac{dM'}{dt} \qquad (B2)$$

The hydrodynamic mass M' may further be expressed as /4/:

$$M' = \frac{\pi}{2} \rho C_v b^2 \qquad (B3)$$

where (see fig. B1)

b = wetted half beam
ρ = density of water
C_v = ratio between hydrodynamic mass of the actual ship and hydrodynamic mass of a circular cylinder of same half beam b.

If (B3) is introduced in (B2) the following expression for F is obtained

$$F_{imp} = M' \frac{dV}{dt} + \frac{\pi \rho V_0}{(1 + \frac{M'}{M})^2} \left[C_v b \frac{db}{dt} + \frac{1}{2} b^2 \frac{dC_v}{dt} \right] \quad (B4)$$

The purpose of this paper is the application to ship-like sections, and according to this M' should not be interpreted as the mass of the strip (section) but rather as an induced mass including the interaction between the strip and the remaining part of the ship. It is therefore reasonable to assume M >> M' which inserted in (B4) gives

$$F_{imp.} (t) = M' \frac{dV}{dt} + \pi \rho V_0 \left[C_v b \frac{dV}{dt} + \frac{1}{2} b^2 \frac{dC_v}{dt} \right] (B5)$$

If the same simplification as in § 2 is employed i.e. $\frac{dV}{dt} \sim 0$, the first term on the right hand side of the equation vanishes, and further it implies that dt = dy V_0 (see fig. 1), hence

$$F_{imp.} (y) = \pi \rho V_0^2 \left[C_v b \frac{db}{dy} + \frac{1}{2} b^2 \frac{dC_v}{dy} \right] \qquad (B6)$$

If this expression is calculated for different section forms it is found that for typical flared forms (sectional area coeff. < ~ 0.7) the contribution to the impact force F_{imp} from the rate of change of C_v is less than about 10 %. This reduces the expression for the impact force on a flared form to (given two-dimensionally as force per length unit)

$$F_{imp.} (y) = \pi \rho b C_v V_0^2 \frac{db}{dy} \qquad (B7)$$

Thus, if the section form is known and a table for C_v is available the two-dimensional impact force F as a function of draught (y) may be estimated.

In order to demonstrate the effect of section form on the impact force fig. B1 has been prepared. A table for C_v is also given, which may be used if eq. (B7) is employed to make rough estimates of bow flare forces.
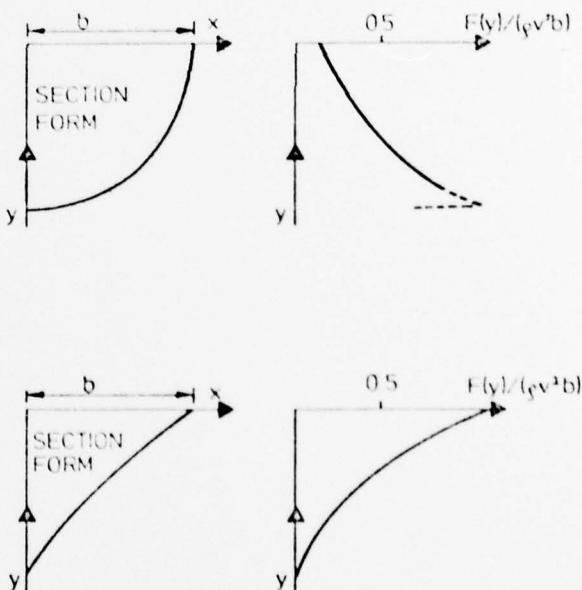

Fig B1. Impact force F per unit length as a function of instantaneous draught y for a full section form (upper figs.) and a flared section form (lower figs.)

39

Section area coeff. (SA) 2d/B	0.5	0.6	0.7	0.8	0.9
0.2	0.90	0.93	0.97	1.01	1.05
0.4	0.85	0.89	0.94	1.01	1.10
0.6	0.82	0.87	0.93	1.02	1.13
0.8	0.80	0.85	0.92	1.02	1.16
1	0.78	0.83	0.91	1.02	1.19
1.5	0.76	0.81	0.89	1.02	1.23
2	0.76	0.80	0.88	1.03	1.26
2.5	0.75	0.79	0.87	1.03	1.26
3	0.75	0.78	0.87	1.03	1.29
4	0.75	0.77	0.86	1.03	1.31

Table 4 Added mass coefficients C_V for Lewis two-parameter forms

Notation

A	—	parameter of Weibull distribution
a	—	wave amplitude
B	—	beam of section (strip)
C_v	—	added mass coefficient
c	—	celerity
d	—	draught of section (strip)
E_{km}	—	kinetic energy
E_x	—	half the area under the response spectrum for $x(t)$
EI	—	bending stiffness module
F_{imp}	—	solid body fluid impact force
F_n	—	Froude number ($= V_s/\sqrt{gL}$)
F_v	—	vertical bow force
g	—	acceleration due to gravity
$H_{1/3}$	—	significant wave height
I	—	moment of inertia including added mass of water
L	—	ship length
M	—	ship (strip) mass
M'	—	added mass of water
M_v	—	vertical bending moment
m	—	parameter of Weibull distribution
η	—	unit vector
P	—	1-Q
Q	—	probability of exceedance
q_i	—	normal coordinate
$\overline{RM}$	—	relative motion
$\overline{RV}$	—	relative velocity
S	—	surface of integration

SA	—	section area coefficient ($= A_s/(Bd)$ where A_s is the cross-sectional area of the section)
s	—	wave steepness
$\bar{T}$	—	average apparent period
T_i	—	inertia coefficient of mode i
T_e	—	period of encounter
T_R	—	peak period of encounter
V	—	immersion velocity
V_0	—	initial immersion velocity
V_s	—	ship speed
a_i	—	damping factor of mode i
Δ	—	displacement
ξ	—	non-dimensional coordinate
ρ	—	density of fluid
σ	—	longitudinal stress in deck
ψ_i	—	mode shape function

References

/1/ CALLUM, J.:
«On the Strength of Fast Cargo Ships».
RINA Meeting April 24, 1974 (London).

/2/ SÆTHRE, J.:
«Stress Measurements on M/S NEPTUNE EMERALD».
DnV Report No. 73-165-C.

/3/ KAPLAN, P. and SARGENT, T. P.:
«Further Studies of Computer Simulation of Slamming and other Wave-induced Vibratory Structural Loadings on Ships in Waves».
Ship Structure Committee, 1972 (SSC-231).

/4/ LEWIS, F. E.:
«The Inertia of the Water Surrounding a Vibrating Ship».
Trans. SNAME, vol. 37, 1929.

/5/ FERDINANDE, V.:
«Theoretical Considerations on the Penetration of a Wedge into the Water».
Int. Shipbldg. Progress v. 13 Apr. 1966, 102–116.

/6/ BISHOP, R. E. D. and EATOCK TAYLOR, R.:
«On Wave-induced Stress in a Ship Executing Symmetric Motions».
Philosophical Transactions of the Royal Society of London 275, 1—32, (1973).

/7/ BISHOP, R. E. D., EATOCK TAYLOR, R. and JACKSON, K. L.:
«On the Structural Dynamics of Ship Hulls in Waves».
The Naval Architect, 3, 257—274, (1973) no. 4.

/8/ HYLARIDES, S.:
«Damping in Propeller Generated Ship Vibrations».
Publication No. 468, Netherlands Ship Model Basin, Wageningen.

/9/ RAYLEIGH, J. W. S.:
The Theory of Sound. Second Edition Dover Publications.
New York 1945. Vol. 1, § 130 p. 189.

INFORMATION FOR CONTRIBUTORS

Contributions should be submitted in accordance with the following instructions to: The Editor, Norwegian Maritime Research, Rådhusgt. 4, Oslo, Sentrum, Norway.

Manuscripts should be in English, typed double spaced with good margins on one side of the paper, and submitted in duplicate. A paper which would occupy more than 8 pages of the Journal (approximately 8000 words), will be returned to the author for abridgement.

The author should state his business connection, the title of his position and his mailing address, and also his telephone number.

Abstract. The text of a paper should be preceded by a summary. This should be short, but should mention all essential points of the paper.

Figures. The drawings for the figures must be submitted on separate sheets, drawn in black india ink in large size and carefully lettered (with the use of stencils). The lettering as well as the details should have proportionate dimensions, so as not to become illegible or unclear after the usual reduction by the printers; in general, the figures should be designed for a reduction factor of two or three. Mathematical symbols should be entered in italics, where appropriate. For photographs, glossy prints are required.

Each figure should have a number and a caption, the captions should be collected on a separate sheet. The appropriate place of the figure should be indicated in the margin.

Tables. Tables should be typed on separate sheets. Each table should have a number and a title. The appropriate places for the insertion of tables should be indicated in the margin.

Formulae. Displayed formulae should be numbered and typed or clearly written by hand. Symbols should be identified in the margin, where they occur for the first time.

References. In the text, reference to other parts of the paper should be made by section (or equation) number, but not by page number.

References to published literature should be quoted in the text in square brackets and grouped at the end of the paper in numerical order. Double spacing must be used throughout.

Journal references should be arranged thus:
1. ANDREWS, J.B., and CUMMINGS, D.E. A Design Procedure for Large Hub Propellers. J. Ship Res. 16(1972):3, pp. 167–73.

Book references should be given as follows:
2. JURAN, J.M., and GRYNA, F.M. Quality Planning and Analysis. New York, McGraw-Hill, 1970.

Proofs. The authors are responsible for seeing that their typescripts are final in form for publication. Proofs are sent to authors in order that they may make sure that the paper has been correctly set up in type, and not that they may add new material or make corrections to the text.